A triple-microstructure hydro-mechanical constitutive damage model for compacted MX80 bentonite pellet/powder mixture

Jin-wen Yang, yu Cui, Nadia Mokni, Hao Wang

Received: 19 April 2023 | Revised: 12 August 2023 | Accepted: 11 October 2023

DOI: 10.1002/nag.3670

RESEARCH ARTICLE

WILEY

A triple-microstructure hydro-mechanical constitutive damage model for compacted MX80 bentonite pellet/powder mixture

Jin-Wen Yang[1,2] | **Yu-jun Cui**[2] | **Nadia Mokni**[3] | **Hao Wang**[2]

[1]China Nuclear Power Engineering Co., Ltd., Beijing, China

[2]Ecole des Ponts ParisTech, Laboratoire Navier/CERMES, Marne-La-Vallée, France

[3]Institut de Radioprotection et de Sûreté Nucléaire (IRSN), PSE-ENV/SEDRE/LETIS, Fontenay-aux-Roses, France

Correspondence
Jin-Wen Yang, China Nuclear Power Engineering Co., Ltd., Beijing, 100840, China.
Email: yangjwd@cnpe.cc

Funding information
China Scholarship Council; Ecole des Ponts ParisTech; Institut de Radioprotection et de SŨreté Nucléaire

Abstract

A triple-microstructure hydro-mechanical constitutive damage model was proposed to describe the hydro-mechanical behaviour of MX80 bentonite pellet/powder mixture, based on the results from a series of suction-controlled oedometer tests and microstructure observations. Emphasis was put on the pellet damage behaviour. The model parameters were determined essentially based on these results. The model response was firstly verified with the obtained oedometer tests. Then, the results of Molinero-Guerra et al. and Darde who carried out suction-controlled oedometer tests and swelling pressure tests on similar bentonite pellet/powder mixture were employed to validate the proposed model. It appeared that the global volume behaviour and the development of swelling pressure with suction of the bentonite mixture could be well reproduced. The model allowed gaining insights into the microstructural evolutions under oedometer loading. The global compression behaviour was governed by the filling of inter-grain pores at unsaturated state, but by the compression of grains themselves at saturated state. Conversely, when wetted under constant-volume condition, inter-grain pores and intra-grain macro-pores were closed, by the swelling of intra-grain micro-pores. Examination of the water-retention property showed that water saturated the intra-grain micro-pores at suction 19 MPa, and then started filling intra-grain macro-pores. When inter-grain pores and intra-grain macro-pores were all closed at suction 0.1 MPa, water finally came back to intra-grain micro-pores. On the whole, the hydro-mechanical behaviour of the bentonite pellet/powder mixture can be well described by the proposed model.

KEYWORDS

bentonite pellet/powder mixture, damage, oedometer compression, suction, triple-microstructure model

1 | INTRODUCTION

Deep geological disposal has been widely recognized as a promising option for high- and intermediate-level radioactive waste. In this concept, bentonite pellet/powder mixture has been envisaged as sealing materials thanks to their

low permeability, high swelling and high radionuclide retardation capacities.[1–5] Under geological disposal conditions, pore water or vapour from host rock would infiltrate the sealing materials, inducing hydration and subsequent swelling. The sealing materials are expected to interact with host rock in the long term. In such wetting and loading processes, these sealing materials may be damaged with cracking. Large cracks may constitute preferential pathways for water, gas and radionuclides, compromising the long-term performance of the geological disposal facilities.[6,7] Thereby, it is essential to account for the damage effect in the description of the hydro-mechanical behaviour of such mixture.

Based on the experimental results, a number of constitutive models have been developed to describe the hydro-mechanical behaviour of compacted bentonite-based materials.[8–17] Gens and Alonso[8] and Alonso et al.[9] proposed the Barcelona Expansive Model (BExM) for unsaturated expansive soils by considering the coupled macro- and micro-structure deformations. This model assumed the microstructure to be elastic and saturated. The authors demonstrated that the coupling function could well describe the effect of micro-structural swelling or shrinkage on the macro-structural deformation.[9] The double-structure BExM for expansive soils has been modified later by many researchers, keeping the microstructure saturated.[18–20] However, Qiao et al.[10,13] pointed out that the microstructure may be unsaturated when the suction is high enough and some plastic deformations may occur at the microstructure scale due to the subdivision of clay particles. An elastoplastic model was thus proposed in the double structure framework (micro- and macro-structure) by introducing traditional plastic deformations at the micro-structure level.[10,13] Wheeler et al.[15] and Musso et al.[21] also considered the elastoplastic behaviour of the microstructure in their models. In this case, the plastic microstructural deformation is assumed to be dependent on both stress and suction.

The double-structure constitutive models are suitable for compacted bentonite-based materials. However, for heterogenous mixtures such as bentonite pellet/ powder mixture, inter-grain (inter-pellet) pores, intra-grain macro- and micro-pores are identified, suggesting a triple-microstructure structure.[7,22,23–25] The double-structure BExM was extended to the triple-microstructure by Cardoso et al.[19] and Zhang.[26] The plastic deformation of inter-grain pores was calculated by considering the coupling mechanism between inter-grain pores and intra-grain pores, the same as the coupling mechanism between intra-grain macro- and micro-pores. Navarro et al.[16,27] proposed a triple-microstructure model to reproduce the hydro-mechanical behaviour of MX80 bentonite pellet mixtures. They assumed that the behaviour of inter-pellet pores was non-linear, isotropic and elastic. However, experimental results evidenced the irreversibility of some deformations of inter-pellet pores under wetting and loading.[7,22,28] Another important characteristic of the bentonite pellet/powder mixture is the damage due to wetting as demonstrated by Molinero-Guerra et al.[29] and Molinero-Guerra.[30] This damage effect was accounted for by Mokni et al.[5] and Zhang et al.[7] However, their damage models only considered the suction effect, while the stress effect was ignored.

In this study, a triple-microstructure hydro-mechanical constitutive damage model was developed, allowing the hydro-mechanical behaviour of MX80 bentonite pellet/powder mixture to be described. A series of suction-controlled oedometer tests were performed on the bentonite mixture. A description of microstructural characteristics of the pellet/powder mixture was given, providing a hydro-mechanical framework for the model development. The damage of pellets due to both wetting and loading was considered. The model parameters were determined essentially based on the test results. The model validation was firstly made based on the oedometer tests carried out in this study. Then, the suction-controlled oedometer tests and swelling pressure tests performed by Molinero-Guerra et al.[22] and Darde[31] on similar bentonite pellet/powder mixture were simulated, further validating the proposed model.

2 | HYDRO-MECHANICAL CHARACTERISATION AND MICROSTRUCTURE OBSERVATION OF BENTONITE PELLET/POWDER MIXTURE

2.1 | Tested material

The tested material is a mixture of MX80 bentonite pellet/powder at a proportion of 80/20 in dry mass. MX80 bentonite comes from Wyoming, USA, provided by the Laviosa MPC company. MX80 bentonite is a sodium bentonite with a montmorillonite content of 80%−92%, other non-clayey inclusions including quartz, calcite and pyrite. The liquid limit is 520%, the plastic limit is 42%, the plastic index is 478%, and the specific gravity is 2.77 Mg/m^3.[32,33]

MX80 bentonite pellets were produced by heavily compacting MX80 bentonite powder in a mould of 7 mm in diameter and 7 mm in height, by Laviosa Minerals. The initial suction ($s = 87.4$ MPa) was measured with a chilled mirror dew point tensiometer (Decagon WP4C) at an initial water content $w = 12.5\%$, which was determined by oven-drying at 105°C for

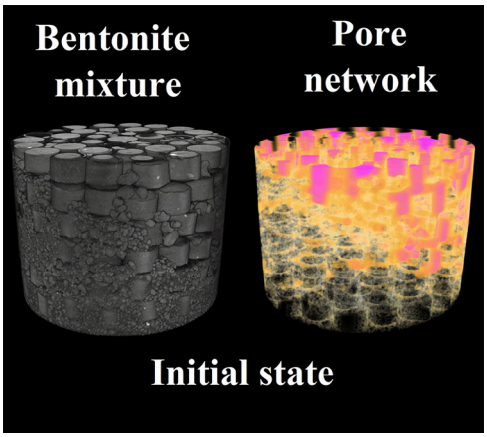

FIGURE 1 μCT images of bentonite pellet/powder mixtures and pore network at initial state.

24 h. The hydrostatic weighing method by immersing waxed sample into desaromatized petroleum was used to determine the pellet volume in the initial state.[34] The initial dry density ρ_d was obtained as 1.91 Mg/m^3, corresponding to an initial void ratio $e = 0.45$. The MX80 bentonite powder was produced by crushing pellets. The pellets and powder could thus be regarded as grains. An initial water content of 5.66% was measured by oven-drying for the powder, corresponding to an initial suction $s = 125.38$ MPa (also by WP4C).

Bentonite pellet/powder mixture was prepared in a cell of 50 mm diameter at a proportion of 80/20 in dry mass. The pellets were axially placed one by one, with the centres of the top and bottom caps in a vertical direction. Once a layer was fully filled with pellets, powder equal to 25% of pellets in dry mass were evenly sprayed between pellets. Six layers in total were placed in the cell with a total sample height around 36 mm. The global dry initial density of the mixture was 1.49 Mg/m^3.

2.2 | Suction-controlled oedometer tests

Suction-controlled oedometer tests were conducted on bentonite pellet/powder mixture samples. The mixture samples were imposed under different suctions from 113 to 4.2 MPa by vapour equilibrium (VET samples) and under zero suction by liquid water circulation (WC samples). The conventional step loading was applied until reaching different target vertical stresses (0.1, 3.2 and 12.8 MPa). Once various target vertical stresses were reached, the outlets and inlets of oedometer cells were closed to stop the vapour or water circulation for the undrained condition. Afterwards, the mixture samples were instantaneously unloaded and extruded from the oedometer cell for later microstructure observations including Mercury Intrusion Porosimetry (MIP) tests and Micro-Computed Tomography (μCT) observations (MIP/μCT). The results from the suction-controlled oedometer tests are used to determine certain model parameters and to validate the proposed model, as shown later.

2.3 | Microstructural characterisation with MIP and μCT

The microstructural characterisation of bentonite pellet/powder mixture was conducted by means of Mercury Intrusion Porosimetry (MIP) tests and Micro-Computed Tomography (μCT) observations. As for μCT observations, the samples were scanned using Skyscanner-1173 with the voltage and current of X-ray sources selected as 130 kV and 61 μA, respectively. The voxel size was 28 μm. After scans, the scanned object was 3D reconstructed by assembling around 1600 horizontal slices using Bruker software NRecon with median noise reduction method. Bruker software CTAn was exploited to post-process these μCT images. The built-in automatic thresholding was used to segment bentonite grains and pores in analysing μCT images.

The μCT images of bentonite pellet/powder mixture and pore network at the initial state are presented in Figure 1. It appears that the bentonite pellet/powder (80/20) mixture sample at initial state mainly comprises pellets. Significant inter-grain pores could be identified from the image of inter-grain pore network. Moreover, more inter-grain pores could

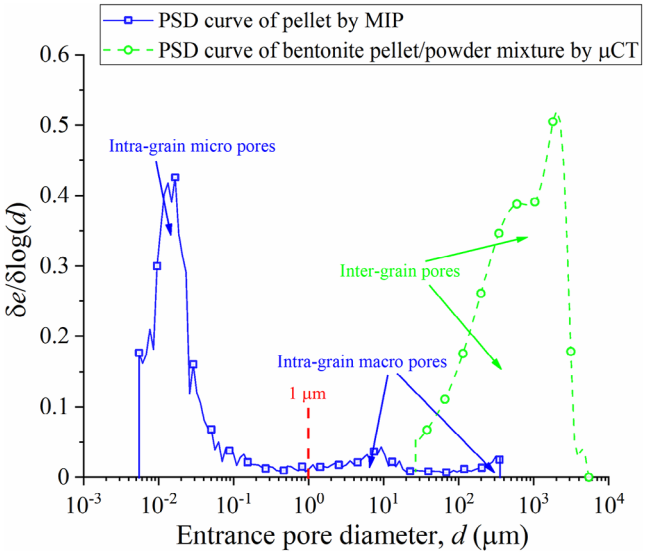

FIGURE 2 Classification of intra-grain micro- and macro-pores and inter-grain pores inside bentonite pellet/powder mixture.

be identified in the top positions than in the middle and bottom positions, since powder grains slid into the bottom through inter-grain pores, in particular during the transportation to the μCT room.

Due to the high volume fraction of pellets to the whole bentonite pellet/powder (80/20) mixture sample at initial state, water was mainly adsorbed by pellets and the stress was transmitted through the pellet skeleton in the bentonite pellet/powder mixture.[35] Thereby, the overall hydro-mechanical behaviour of the bentonite mixture was rather governed by pellets. The MIP tests were conducted on several freeze-dried pellets at the initial state by a porosimeter of Micromeritics AutoPore IV 9500, with the pore entrance diameters from 344 μm to 5.5 nm to be identified. The μCT-detection Pore Size Distribution (PSD) curve of bentonite mixture sample was obtained by the method of Yang et al.[36] The MIP-detection PSD curve of pellet and μCT-detection PSD curve of bentonite mixture sample are depicted in Figure 2. Three pore structures can be identified, representing intra-grain micro- and macro-pores inside pellets and powder grains and inter-grain pores between pellets and powder grains. Note that the sizes of intra-grain macro-pores were larger than 1 μm, whereas the sizes of intra-grain micro-pores were smaller than 1 μm. The pores that surround pellets and powder grains were classified into inter-grain pores.

The MIP results of pellets taken from bentonite mixture samples unloaded from various imposed suctions and applied loads are presented in Figure 3, in terms of cumulative and density function curves. The cumulative curves were well ordered with respect to the suction for the vertical stress σ_v of 0.1 and 3.2 MPa (Figure 3A,B): the curve for a lower suction lies above the curve for a higher suction. By contrast, for the σ_v of 12.8 MPa (Figure 3C), the difference between the cumulative curves became limited, showing that loading narrowed the difference. The density function curves were characterised by a bimodal porosity for all the VET samples, whereas by a tri-modal porosity for all the WC samples except S0L12.8.

The water distribution within pores in grains was studied with MIP results using the method proposed by Wang et al.,[37] who assimilated the mercury cumulative intrusion to the air intrusion process. The maximum size of water-filled pores d_{wm} could be obtained and is also presented in density function curves of Figure 3. It appears that the intra-grain micro-pores were unsaturated at suctions higher than 25 MPa, while saturated at suctions smaller than 9 MPa, except S4.2L3.2 and S4.2L12.8. On the contrary, all the intra-grain macro-pores were unsaturated for all suctions.

2.4 | Swelling and damage mechanisms

As mentioned previously, three pore structures including intra-grain micro- and macro-pores and inter-grain pores, were identified in bentonite pellet/powder mixture. The variations of void ratios of inter-grain, intra-grain macro- and intra-grain micro- pores (e^{inter}, e_M^{intra} and e_m^{intra}) with suction s and vertical stress σ_v are quantitatively depicted in Figure 4. e_m^{intra} is the difference between e_T^{intra} and e_M^{intra} and e^{inter} is the difference between e_T and e_T^{intra}. The values of e_T^{intra} and e_T

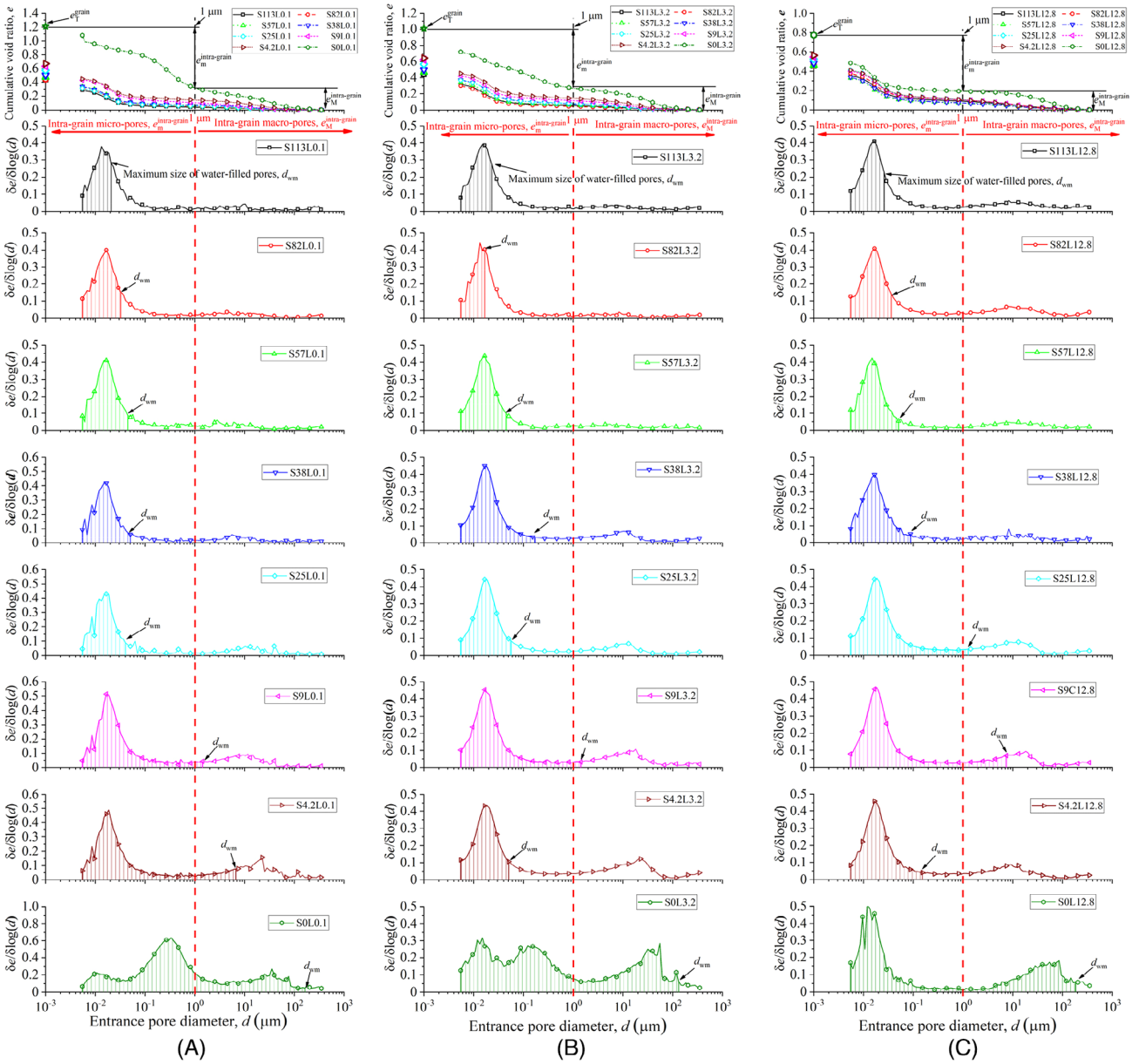

FIGURE 3 PSD curves of pellets taken out from bentonite mixtures instantaneously unloaded from various imposed suctions and different target vertical stresses: (A) $\sigma_v = 0.1$ MPa; (B) $\sigma_v = 3.2$ MPa; (C) $\sigma_v = 12.8$ MPa.

could be obtained from Figures 3 and 10A, respectively. During wetting, both e_M^{intra} and e_m^{intra} increased with s decrease, contrary to the decreasing e^{inter}, indicating the filling of inter-grain pores by the swelling of pellets and powder grains. This suggests that inter-grain and intra-grain pores are coupled. During loading, Δe^{inter} was larger than Δe_M^{intra} and Δe_m^{intra} for the VET samples, but much smaller than Δe_M^{intra} and Δe_m^{intra} for the WC samples. This suggests that the compaction of bentonite mixture was mainly controlled by the filling of inter-grain pores for the VET samples, but by the compression of intra-grain pores for the WC samples. As for the intra-grain pores, Δe_m^{intra} under each loading level increased with s decrease because of the wetting-reduced swelling of pellets and powder grains.

Accounting for the damage behaviour of bentonite pellet/powder mixture under wetting or/and loading is indispensable in the constitutive modelling. The intra-grain macro-pores could be regarded as cracks.[5] It appears that e_M^{intra} increased with σ_v increase for $s \geq 82$ MPa, indicating the consistent crack generation during loading (Figure 4). By contrast, for $s = 4.2$ MPa, e_M^{intra} decreased insignificantly at low loads, but decreased remarkably at high loads, reflecting the crack closure. e_M^{intra} appears almost unchanged for s between 57 and 9 MPa, suggesting the limited cracking behaviour in this suction range. Thereby, both suction and stress affect the damage behaviour of bentonite pellet/powder mixture.

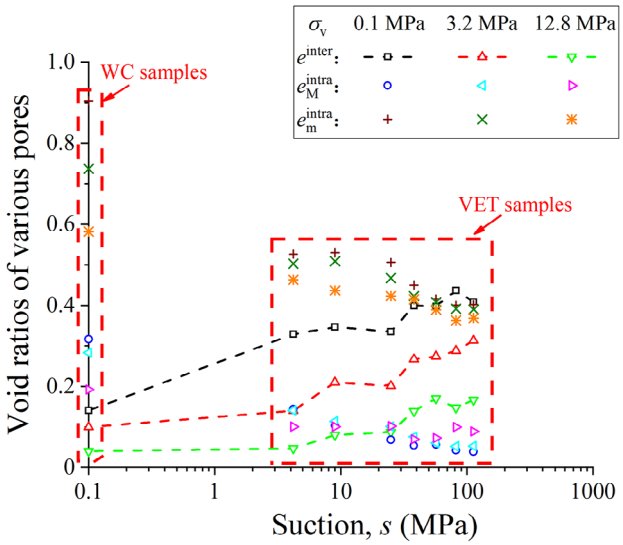

FIGURE 4 Variations of inter-grain, intra-grain macro- and intra-grain micro-void ratios (e^{inter}, e_M^{intra} and e_m^{intra}) with suction and stress.

3 | TRIPLE-MICROSTRUCTURE HYDRO-MECHANICAL CONSTITUTIVE DAMAGE MODEL

3.1 | Basic assumptions

In order to appropriately account for the three pore structural levels of the studied mixture upon wetting and loading, a triple-microstructure hydro-mechanical constitutive damage model is proposed. Given the different strain responses to suction and stress variations at the three pore structures (Figure 4), two independent stress variables are considered: mean net stress and suction. The model assumes that the mechanical behaviours of the three pore structural levels are elastoplastic. This assumption is based on the results of Zhang et al.[7] who identified some irreversible deformations from all the three pore structures upon wetting/drying/re-wetting on single MX80 bentonite 7-mm pellets.

For simplicity, the following assumptions are adopted:

1. Mechanical, hydraulic and chemical equilibriums are reached between intra-grain and inter-grain pores, and between intra-grain macro- and micro-pores.
2. No mass, entropy or internal energy are transferred among the solid, liquid and gas phases. All the three phases have the same and constant temperature.
3. The solid phase is uncompressible. All the deformations of three pore structures are considered as volumetric.

3.1.1 | Structural equations

The mixture total void ratio e_T is the sum of the void ratios of intra-grain micro and macro-pores and inter-grain pores (e_m^{intra}, e_M^{intra} and e^{inter}), as shown in Equation (1):

$$e_T = e_m^{intra} + e_M^{intra} + e^{inter} \tag{1}$$

where e_m^{intra}, e_M^{intra} and e^{inter} can be calculated with the following equations:

$$e_m^{intra} = \frac{V_m^{intra}}{V_s}, \quad e_M^{intra} = \frac{V_M^{intra}}{V_s} \text{ and } e^{inter} = \frac{V^{inter}}{V_s} \tag{2}$$

where V_m^{intra}, V_M^{intra} and V^{inter} are the volume of intra-grain micro-, intra-grain macro- and inter-grain pores. e_m^{intra} and e_M^{intra} constitute the total void ratio of grain e_T^{intra}:

$$e_T^{intra} = e_m^{intra} + e_M^{intra} \tag{3}$$

The volumetric strains corresponding to the intra-grain micro- and macro-pores as well as inter-grain pores ($\varepsilon_{\mathrm{m}}^{\mathrm{intra}}$, $\varepsilon_{\mathrm{M}}^{\mathrm{intra}}$ and $\varepsilon^{\mathrm{inter}}$) are defined by Equation (4):

$$\varepsilon_{\mathrm{m}}^{\mathrm{intra}} = \frac{\Delta e_{\mathrm{m}}^{\mathrm{intra}}}{1+e_{\mathrm{T}}},\ \varepsilon_{\mathrm{M}}^{\mathrm{intra}} = \frac{\Delta e_{\mathrm{M}}^{\mathrm{intra}}}{1+e_{\mathrm{T}}} \text{ and } \varepsilon^{\mathrm{inter}} = \frac{\Delta e^{\mathrm{inter}}}{1+e_{\mathrm{T}}} \tag{4}$$

The corresponding total volumetric strain ε_{T} is:

$$\varepsilon_{\mathrm{T}} = \varepsilon_{\mathrm{m}}^{\mathrm{intra}} + \varepsilon_{\mathrm{M}}^{\mathrm{intra}} + \varepsilon^{\mathrm{inter}} \tag{5}$$

3.1.2 | Hydraulic constitutive equations

The saturation degrees of intra-grain micro- and macro-pores ($S_{\mathrm{rm}}^{\mathrm{intra}}$ and $S_{\mathrm{rM}}^{\mathrm{intra}}$) are defined as:

$$S_{\mathrm{rm}}^{\mathrm{intra}} = \frac{e_{\mathrm{wm}}^{\mathrm{intra}}}{e_{\mathrm{m}}^{\mathrm{intra}}} \text{ and } S_{\mathrm{rM}}^{\mathrm{intra}} = \frac{e_{\mathrm{wM}}^{\mathrm{intra}}}{e_{\mathrm{M}}^{\mathrm{intra}}} \tag{6}$$

where $e_{\mathrm{wm}}^{\mathrm{intra}}$ and $e_{\mathrm{wM}}^{\mathrm{intra}}$ are the water void ratios for intra-grain micro- and macro-pores, respectively, calculated as:

$$e_{\mathrm{wm}}^{\mathrm{intra}} = \frac{V_{\mathrm{V,wm}}^{\mathrm{intra}}}{V_{\mathrm{s}}} \text{ and } e_{\mathrm{wM}}^{\mathrm{intra}} = \frac{V_{\mathrm{V,wM}}^{\mathrm{intra}}}{V_{\mathrm{s}}} \tag{7}$$

where $V_{\mathrm{V,wm}}^{\mathrm{intra}}$ and $V_{\mathrm{V,wM}}^{\mathrm{intra}}$ are the volumes of water stored in the intra-grain micro- and intra-grain macro-pores, respectively. The saturation degree of whole grain $S_{\mathrm{r}}^{\mathrm{intra}}$ is:

$$S_{\mathrm{r}}^{\mathrm{intra}} = \frac{e_{\mathrm{w}}}{e_{\mathrm{T}}^{\mathrm{intra}}} = \frac{e_{\mathrm{m}}^{\mathrm{intra}}}{e_{\mathrm{T}}^{\mathrm{intra}}} S_{\mathrm{rm}}^{\mathrm{intra}} + \frac{e_{\mathrm{M}}^{\mathrm{intra}}}{e_{\mathrm{T}}^{\mathrm{intra}}} S_{\mathrm{rM}}^{\mathrm{intra}} \tag{8}$$

The saturation degree of mixture S_{r} is calculated from $S_{\mathrm{r}}^{\mathrm{intra}}$, as water is stored in grains after unloading.

$$S_{\mathrm{r}} = \frac{e_{\mathrm{w}}}{e_{\mathrm{T}}} = \frac{e_{\mathrm{T}}^{\mathrm{intra}}}{e_{\mathrm{T}}} S_{\mathrm{r}}^{\mathrm{intra}} \tag{9}$$

The water retention model adopted for the three pore structural levels is:

$$S_{\mathrm{r}}(s,p) = \left[1 + \left(\frac{\left(e_0 - \alpha_{\mathrm{p}}\ln\left(1+p/p_{\mathrm{r}}\right) - \alpha_{\mathrm{s}}\ln\left(1+s/p_{\mathrm{atm}}\right)\right)^{m_4}}{m_3\left(1+p/p_{\mathrm{atm}}\right)^{m_5}} s\right)^{m_2}\right]^{-m_1} \tag{10}$$

where p_{r} is a reference pressure and e_0 is the initial void ratio; α_{p} represents soil compressibility with respect to net mean stress; α_{s} represents soil compressibility with respect to suction; m_1, m_2, m_3, m_4 and m_5 are soil parameters. According to Zhou and Ng,[38] parameters m_1, m_2 and m_4 satisfy the following relationship (Equation (11)):

$$m_1 m_2 m_4 = 1 \tag{11}$$

This water retention model proposed by Zhou and Ng[38] considers the stress effect on the retention properties of the material. This dependency was found to play an important role in the water retention behaviour of the mixture.[39] The parameters of the water-retention model will be determined by fitting the model with the experimental data.

Table 1 summarises the equations for the basic assumptions.

TABLE 1 Summary of the equations for the basic assumptions.

Name	Equation	Code
Total void ratio	$e_T = e_m^{intra} + e_M^{intra} + e^{inter}$	(1)
Void ratios	$e_m^{intra} = \frac{V_{Vm}^{intra}}{V_s}$ $e_M^{intra} = \frac{V_{VM}^{intra}}{V_s}$ $e^{inter} = \frac{V_V^{inter}}{V_s}$	(2)
Total grain void ratio	$e_T^{intra} = e_m^{intra} + e_M^{intra}$	(3)
Volumetric deformations	$\varepsilon_m^{intra} = \frac{\Delta e_m^{intra}}{1+e_T}$ $\varepsilon_M^{intra} = \frac{\Delta e_M^{intra}}{1+e_T}$ $\varepsilon_T^{inter} = \frac{\Delta e^{inter}}{1+e_T}$	(4)
Total deformation	$\varepsilon_T = \varepsilon_m^{intra} + \varepsilon_M^{intra} + \varepsilon^{inter}$	(5)
Degree of saturation of intra-grain micro- and macro-pores	$S_{rm}^{intra} = \frac{e_{wm}^{intra}}{e_m^{intra}}$ $S_{rM}^{intra} = \frac{e_{wM}^{intra}}{e_M^{intra}}$	(6)
Void ratio occupied by water	$e_{wm}^{intra} = \frac{V_{V,wm}^{intra}}{V_s}$ $e_{wM}^{intra} = \frac{V_{V,wM}^{intra}}{V_s}$	(7)
Degree of saturation of grain	$S_r^{intra} = \frac{e_w}{e_T^{intra}} = \frac{e_m^{intra}}{e_T^{intra}} S_{rm}^{intra} + \frac{e_M^{intra}}{e_T^{intra}} S_{rM}^{intra}$	(8)
Degree of saturation of mixture	$S_r = \frac{e_w}{e_T} = \frac{e_T^{intra}}{e_T} S_r^{intra}$	(9)

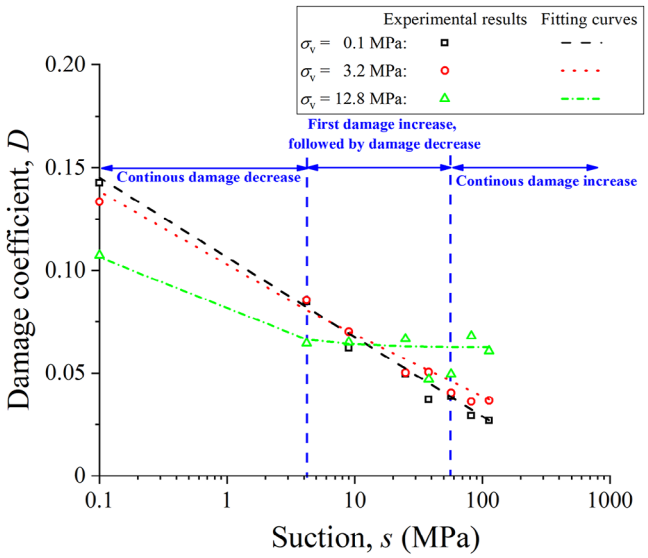

FIGURE 5 Damage coefficient versus suction.

3.2 | Damage model

A distinct damage coefficient of pellets considering the volume of clay solid is proposed (Equation (12)):

$$D = \frac{V_M^{intra}}{V_s + V_M^{intra} + V_m^{intra}} = \frac{e_M^{intra}}{1 + e_T^{intra}} \tag{12}$$

The intra-grain macro-pores were regarded as cracks. Indeed, the damage coefficient was determined by the percentage of intra-grain macro-pores in the whole volume. V_M^{intra} and $V_s + V_M^{intra} + V_m^{intra}$ are divided by V_s, yielding e_M^{intra} and $1+e_T^{intra}$, respectively. Accordingly, the damage coefficient is calculated by dividing e_M^{intra} by $1+e_T^{intra}$ and is presented in Figure 5. It appears that during wetting, the smaller the suction, the larger the D, for all suctions. During loading, the D value continuously increased for suctions larger than 57 MPa. On the contrary, for suctions smaller than 4.2 MPa, the D value decreased during loading. As for suctions smaller than 38 MPa and larger than 9 MPa, the D value grew up when the vertical stress was applied from 0.1 to 3.2 MPa, but decreased when the vertical stress was applied from 3.2 to 12.8 MPa. Change in wetting-induced damage $\Delta D^{wetting}$ and change in loading-induced damage $\Delta D^{loading}$ were extracted from the damage coefficients to clarify the effects of wetting and loading on damage. $\Delta D^{wetting}$ is defined as the difference between the damage coefficient at a given suction under the initial load $D_{L0.1}$ and that at initial state $D_{S113L0.1}$ that characterised

the fabrication-induced damage, yielding Equation (13):

$$\Delta D^{\text{wetting}} = D_{\text{L0.1}} - D_{\text{S113L0.1}} \tag{13}$$

$D_{\text{S113L0.1}}$ was 0.027. The $\Delta D^{\text{loading}}$ was defined as the difference between the damage coefficient under a given load ($D_{\text{L3.2}}$ and $D_{\text{L12.8}}$) and that under the initial load ($D_{\text{L0.1}}$) at a given suction, resulting in Equation (14):

$$\Delta D^{\text{loading}} = D_{\text{L3.2}} - D_{\text{L0.1}} \text{ or } \Delta D^{\text{loading}} = D_{\text{L12.8}} - D_{\text{L0.1}} \tag{14}$$

Equations (15) and (16) are proposed to describe $\Delta D^{\text{wetting}}$ and $\Delta D^{\text{loading}}$, respectively:

$$\Delta D^{\text{wetting}}(s) = ms^n \tag{15}$$

$$\Delta D^{\text{loading}}(s,p) = c\ln(as - p_{\text{atm}})\exp(bp+1) + h \tag{16}$$

where parameters m, n, a, b, c and h are determined by fitting, equal to 0.19, −0.78, 0.060, 0.16, 0.0015 and 0.0056, respectively. p_{atm} is the atmosphere pressure (0.1 MPa). As for the physical meanings, m and n controlled the suction effect on the wetting-induced damage. a and b controlled the suction effect and the stress effect on the loading-induced damage, respectively. Summing the initial damage coefficient $D_{\text{S113L0.1}}$ and Equations (15) and (16), the total damage coefficient D is obtained through Equation (17):

$$D(s,p) = 0.027 + 0.19s^{-0.78} + 0.0015\ln(0.060s - 0.101)\exp(0.16p+1) + 0.0056 \tag{17}$$

As observed from Figure 5, the fitting curves matched well with the experimental D.

3.3 | Mechanical constitutive equations

3.3.1 | Intra-grain micro-pore level

The total incremental strain for intra-grain micro-pores $\Delta\varepsilon_{\text{m}}^{\text{intra}}$ is the sum of the elastic part $\Delta\varepsilon_{\text{m}}^{\text{e,intra}}$ and the plastic part $\Delta\varepsilon_{\text{m}}^{\text{p,intra}}$:

$$\Delta\varepsilon_{\text{m}}^{\text{intra}} = \Delta\varepsilon_{\text{m}}^{\text{e,intra}} + \Delta\varepsilon_{\text{m}}^{\text{p,intra}} \tag{18}$$

It is assumed that the intra grain microstructural level is controlled by two independent variables, mean net stress (p) and suction (s), as follows:

$$\Delta\varepsilon_{\text{m}}^{\text{e,intra}} = \frac{\Delta p}{(1-D)K_{\text{pm}}^{\text{intra}}} + \frac{\Delta s}{(1-D)K_{\text{sm}}^{\text{intra}}} \tag{19}$$

where D is the damage coefficient, $K_{\text{pm}}^{\text{intra}}$ and $K_{\text{sm}}^{\text{intra}}$ are the bulk moduli for the intra-grain micro-pores for stress and suction, respectively, and are calculated by Equation (20):

$$K_{\text{pm}}^{\text{intra}} = \frac{(1+e_{\text{T}})p}{\kappa_{\text{pm}}^{\text{intra}}} \text{ and } K_{\text{sm}}^{\text{intra}} = \frac{(1+e_{\text{T}})s}{\kappa_{\text{sm}}^{\text{intra}}} \tag{20}$$

where $\kappa_{\text{pm}}^{\text{intra}}$ is the elastic compression index in $e_{\text{M}}^{\text{intra}}$-ln$p$ plane and $\kappa_{\text{sm}}^{\text{intra}}$ is the elastic parameter for intra-grain micro-pores with suction changes.

To describe the plastic strain, the plastic model of Musso et al.[15] is adopted. Two yield curves are introduced for the description of the plastic strains—one is suction decrease (SD) or suction increase (SI) yield curve and another is loading-collapse (LC) yield curve. The former is related to the irreversible change of water ratio and the latter is related to mechanical straining. Wheeler et al.[21] and Musso et al.[15] pointed out that if yielding occurs directly on the SI, the water ratio changes following the drying water-retention curves (WRC), accompanied by the hardening of the LC, while direct

yielding on the SD causes water ratio changes following the wetting WRC, together with the softening of the LC. If yielding occurs on the LC, it produces plastic volumetric strains with a coupled outward movement of the SI or inward movement of the SD.[15] These yield curves are expressed as:

$$\mathrm{LC}:\ p = p_0\ \mathrm{SI}:\ s = s_\mathrm{I}\ \mathrm{SD}:\ s = s_\mathrm{D} \tag{21}$$

where s_I and s_D are the suctions on SI and SD, respectively. $p_0(s)$ is the pre-consolidation pressure for the whole bentonite mixture. Since the overall hydro-mechanical behaviour of the bentonite mixture is rather governed by pellets, it can be reasonably deduced that the pellets shared the same pre-consolidation pressures with the whole bentonite mixture samples at various suctions. Thus, $p_0(s)$ is adopted for the intra-grain micro- and macro-pores and inter-grain pores.

The movements of SI and the SD are the same:

$$\frac{\Delta s_\mathrm{I}}{s_\mathrm{I}} = \frac{\Delta s_\mathrm{D}}{s_\mathrm{D}} = \frac{\Delta s}{s} \tag{22}$$

Musso et al.[15] proposed the following hardening law for the yielding related to to SI or SD:

$$\Delta p_0 = h_{\mathrm{LC,imi}} p_0 \left(\frac{\Delta s}{s}\right) \tag{23}$$

where $h_{\mathrm{LC,imi}}$ is the parameter that controls the softening or hardening of the LC curve due to SD or SI yielding for the intra-grain micro-pores. The incremental plastic volumetric strain for intra-grain micro-pores due to yielding of the LC curve $\Delta\varepsilon_\mathrm{m}^{\mathrm{p,intra}}$ is:

$$\Delta \varepsilon_\mathrm{m}^{\mathrm{p,intra}} = \frac{\lambda_\mathrm{m}^{\mathrm{intra}}(\mathrm{s}) - \kappa_\mathrm{pm}^{\mathrm{intra}}}{1 + e_\mathrm{T}} \frac{\Delta p_0}{p_0} \tag{24}$$

where $\lambda_\mathrm{m}^{\mathrm{intra}}(s)$ is the slope of the virgin consolidation line in $e_\mathrm{m}^{\mathrm{intra}}$-ln$p$ plane at a given suction s. In this case, the hardening law was given by Musso et al.[15]:

$$\Delta s = h_{\mathrm{s,imi}}\, s \frac{\Delta p_0}{p_0} \tag{25}$$

where $h_{\mathrm{s,imi}}$ is the parameter that controls the inward movement of SD yield curve or outward movement of SI yield curve for the intra-grain micro-pores. The general expression for $\Delta\varepsilon_\mathrm{m}^{\mathrm{p,intra}}$ can be derived through Equations (22)–(25)[15]:

$$\Delta \varepsilon_\mathrm{m}^{\mathrm{p,intra}} = \frac{\lambda_\mathrm{m}^{\mathrm{intra}}(\mathrm{s}) - \kappa_\mathrm{pm}^{\mathrm{intra}}}{(1 + e_\mathrm{T})\left(1 - h_{\mathrm{s,imi}} h_{\mathrm{LC,imi}}\right)} \left(\frac{\Delta p_0}{p_0} - h_{\mathrm{LC,imi}} \left(\frac{\Delta s}{s}\right)\right) \tag{26}$$

The saturation degree of intra-grain micro-pores $S_\mathrm{rm}^{\mathrm{intra}}$ and the power parameter $\alpha_\mathrm{m}^{\mathrm{intra}}$ are introduced in Equation (26) to control the suction contribution. The larger the water occupation, the larger the suction contribution. If the $(S_\mathrm{rm}^{\mathrm{intra}})^{\alpha_\mathrm{m}^{\mathrm{intra}}}$ is equal to zero, the suction contribution is zero. The $\Delta\varepsilon_\mathrm{m}^{\mathrm{p,intra}}$ is updated, as follows (Equation (27)):

$$\Delta \varepsilon_\mathrm{m}^{\mathrm{p,intra}} = \frac{\lambda_\mathrm{m}^{\mathrm{intra}}(\mathrm{s}) - \kappa_\mathrm{pm}^{\mathrm{intra}}}{(1 + e_\mathrm{T})\left(1 - h_{\mathrm{s,imi}} h_{\mathrm{LC,imi}}\right)} \left(\frac{\Delta p_0}{p_0} - h_{\mathrm{LC,imi}} \left(\frac{(S_\mathrm{rm}^{\mathrm{intra}})^{\alpha_\mathrm{m}^{\mathrm{intra}}} \Delta s}{s}\right)\right) \tag{27}$$

Considering that the smaller the suction, the larger the strain increment,[7] $h_{\mathrm{LC,imi}}$ is defined as a function of suction (Equation (28)):

$$h_{\mathrm{LC,imi}} = h_1 \exp\left(-h_2 s\right) \tag{28}$$

where h_1 and h_2 are parameters related to $h_{\mathrm{LC,imi}}$. According to Wheeler et al.[21], $h_{\mathrm{s,imi}}$ and $h_{\mathrm{LC,imi}}$ satisfied the following relationship:

$$h_{\mathrm{s,imi}} h_{\mathrm{LC,imi}} < 1 \tag{29}$$

The pre-consolidation pressure for mixture at a given suction $p_0(s)$ could be calculated with Equation (30):

$$p_0(s) = p_c \left(\frac{p_0^*}{p_c}\right)^{\left(\frac{\lambda_T(0)-\kappa_T}{\lambda_T(s)-\kappa_T}\right)} \tag{30}$$

where p_c is the reference pressure for the mixture, p_0^* is the saturated pre-consolidation pressure of mixture, κ_T is the elastic compression index in e_T-ln$p$ plane and $\lambda_T(s)$ is the slope of the virgin consolidation line in e_T-ln$p$ plane at a given suction s.

Specifically, when the pre-consolidation pressure is exceeded at constant suction, Equation (27) is reduced to Equation (31):

$$\Delta \varepsilon_{vm}^{p,intra} = \frac{\lambda_m^{intra}(s) - \kappa_{pm}^{intra}}{1+e_T} \frac{\Delta p}{p} \tag{31}$$

where p is the current mean net stress.

3.3.2 | Intra-grain macro-pore level

The framework of the BExM is adopted for the intra-grain macro-pore level. The total incremental strain for intra-grain macro-pores $\Delta\varepsilon_M^{intra}$ is the sum of the elastic and plastic volumetric strains ($\Delta\varepsilon_M^{e,intra}$ and $\Delta\varepsilon_M^{p,intra}$):

$$\Delta \varepsilon_M^{intra} = \Delta\varepsilon_M^{e,intra} + \Delta\varepsilon_M^{p,intra} \tag{32}$$

For the elastic part, $\Delta\varepsilon_M^{e,intra}$ can be calculated with Equation (33), with incorporating the damage coefficient D:

$$\Delta \varepsilon_M^{e,intra} = \frac{\Delta p}{(1-D)K_{pM}^{intra} p} + \frac{\Delta s}{(1-D)K_{sM}^{intra} s} \tag{33}$$

where K_{pM}^{intra} and K_{sM}^{intra} are the bulk moduli for intra-grain macro-pores for stress and suction, which could be obtained with:

$$K_{pM}^{intra} = \frac{(1+e_T)p}{\kappa_M^{intra}} \text{ and } K_{sM}^{intra} = \frac{(1+e_T)s}{\kappa_{sM}^{intra}} \tag{34}$$

where κ_{pM}^{intra} is the elastic compression index in e_M^{intra}-ln$p$ plane and κ_{sM}^{intra} is the elastic parameter for the intra-grain macro-pores with suction changes. The plastic strain at the level of intra-grain micro-pores is induced by SD or SI yielding ($\Delta\varepsilon_M^{p,SD,intra}$ or $\Delta\varepsilon_M^{p,SI,intra}$) and by LC yielding $\Delta\varepsilon_M^{p,LC,intra}$, as follows (Equation (35)):

$$\Delta \varepsilon_M^{p,intra} = \Delta\varepsilon_M^{p,SD,intra} + \Delta\varepsilon_M^{p,SI,intra} + \Delta\varepsilon_M^{p,LC,intra} \tag{35}$$

The SD and SI yield curves are assumed to be always activated.[40]

The volumetric plastic strain of intra-grain macro-pores is induced by the swelling or shrinkage of the intra-grain micro-pores with suction changes, through the coupling mechanism between the two pore structures.[21] As in the BExM, $\Delta\varepsilon_M^{p,SD,intra}$ or $\Delta\varepsilon_M^{p,SI,intra}$ can be calculated with considering the coupling function between intra-grain micro- and macro-pores f_{MD}^{intra} or f_{MI}^{intra}[9,19,40]:

$$\begin{aligned} \Delta\varepsilon_M^{p,SD,intra} &= f_{MD}^{intra}\,\Delta\varepsilon_m^{intra} \\ \Delta\varepsilon_M^{p,SI,intra} &= f_{MI}^{intra}\,\Delta\varepsilon_m^{intra} \end{aligned} \tag{36}$$

where $\Delta\varepsilon_m^{intra}$ is the total incremental volumetric strain for intra-grain micro-pores, obtained by Equation (18); f_{MD}^{intra} and f_{MI}^{intra} are the coupling functions between the intra-grain micro- and macro-pores in cases of suction decrease and suction

increase, respectively. A common expression $f_{\mathrm{M}}^{\mathrm{intra}}$ proposed by Zhang[26] is used for $f_{\mathrm{MD}}^{\mathrm{intra}}$ and $f_{\mathrm{MI}}^{\mathrm{intra}}$, which is:

$$f_{\mathrm{M}}^{\mathrm{intra}} = \frac{a_{\mathrm{M}}^{\mathrm{intra}}}{1 + \exp\left(b_{\mathrm{M}}^{\mathrm{intra}} + c_{\mathrm{M}}^{\mathrm{intra}} \frac{p}{p_0(s)}\right)} \tag{37}$$

where parameters $a_{\mathrm{M}}^{\mathrm{intra}}$, $b_{\mathrm{M}}^{\mathrm{intra}}$ and $c_{\mathrm{M}}^{\mathrm{intra}}$ are different in cases of SD and SI. $p_0(s)$ is calculated with Equation (19) as mentioned previously.

$\Delta\varepsilon_{\mathrm{M}}^{\mathrm{p,LC,intra}}$ is calculated based on the coupled movement of the LC curve due to SD or SI yielding, as follows:

$$\Delta\,\varepsilon_{\mathrm{M}}^{\mathrm{p,LC,intra}} = \frac{\lambda_{\mathrm{M}}^{\mathrm{intra}}(\mathrm{s}) - \kappa_{\mathrm{pM}}^{\mathrm{intra}}}{(1+e_{\mathrm{T}})\left(1 - h_{\mathrm{s,ima}} h_{\mathrm{LC,ima}}\right)} \left(\frac{\Delta p_0}{p_0} - h_{\mathrm{LC,ima}} \left(\frac{(S_{\mathrm{rM}}^{\mathrm{intra}})^{\alpha_{\mathrm{M}}^{\mathrm{intra}}} \Delta s}{s}\right)\right) \tag{38}$$

where $\lambda_{\mathrm{M}}^{\mathrm{intra}}(\mathrm{s})$ is the slope of the virgin consolidation line in $e_{\mathrm{M}}^{\mathrm{intra}}$-ln$p$ plane at a given suction s. $S_{\mathrm{rM}}^{\mathrm{intra}}$ is the saturation degree of intra-grain macro-pores and $\alpha_{\mathrm{M}}^{\mathrm{intra}}$ is the power parameter, controlling the suction contribution. If the $(S_{\mathrm{rM}}^{\mathrm{intra}})^{\alpha_{\mathrm{M}}^{\mathrm{intra}}}$ equals zero, the suction contribution is zero. $h_{\mathrm{s,ima}}$ is the parameter that controls the SD or SI yielding, and $h_{\mathrm{LC,ima}}$ is the function with the variable of suction, which controls the coupled movement of the LC curve due to SD or SI yielding for the intra-grain micro-pores. The expression of $h_{\mathrm{LC,ima}}$ is Equation (39):

$$h_{\mathrm{LC,ima}} = h_3 \exp(-h_4 s) \tag{39}$$

where h_3 and h_4 are parameters related to $h_{\mathrm{LC,ima}}$. $h_{\mathrm{s,ima}}$ and $h_{\mathrm{LC,ima}}$ also satisfy the following relationship[21]:

$$h_{\mathrm{s,ima}} h_{\mathrm{LC,ima}} < 1 \tag{40}$$

In the case of suction-controlled oedometer loading, when the mean net stress (vertical stress) exceeds the pre-consolidation stress, $\Delta\varepsilon_{\mathrm{M}}^{\mathrm{p,LC,intra}}$ is reduced to Equation (41):

$$\Delta\,\varepsilon_{\mathrm{M}}^{\mathrm{p,LC,intra}} = \frac{\lambda_{\mathrm{M}}^{\mathrm{intra}}(\mathrm{s}) - \kappa_{\mathrm{pM}}^{\mathrm{intra}}}{1+e_{\mathrm{T}}} \frac{\Delta p}{p} \tag{41}$$

3.3.3 | Inter-grain pore level

The framework of the BExM is adopted for describing the deformation of inter-grain pores. The total incremental strain for inter-grain pores $\Delta\varepsilon^{\mathrm{inter}}$ is the sum of the elastic part $\Delta\varepsilon^{\mathrm{e,inter}}$ and the plastic part $\Delta\varepsilon^{\mathrm{p,inter}}$:

$$\Delta\,\varepsilon^{\mathrm{inter}} = \Delta\varepsilon^{\mathrm{e,inter}} + \Delta\varepsilon^{\mathrm{p,inter}} \tag{42}$$

As for the inter-grain pores, the increment of elastic volumetric strain for the inter-grain pores $\Delta\varepsilon^{\mathrm{e,inter}}$ is:

$$\Delta\,\varepsilon^{\mathrm{e,inter}} = -\frac{\Delta p}{K_{\mathrm{p}}^{\mathrm{inter}}} - \frac{\Delta s}{K_{\mathrm{s}}^{\mathrm{inter}}} \tag{43}$$

where the bulk moduli of inter-grain pores for respectively stress and suction, $K_{\mathrm{p}}^{\mathrm{inter}}$ and $K_{\mathrm{s}}^{\mathrm{inter}}$, can be calculated with Equation (44). Note that the negative sign is adopted due to the filling of these pores during wetting and loading, as mentioned previously in Section 2.3.

$$K_{\mathrm{p}}^{\mathrm{inter}} = \frac{(1+e_{\mathrm{T}})\,p}{\kappa_{\mathrm{p}}^{\mathrm{inter}}} \text{ and } K_{\mathrm{s}}^{\mathrm{inter}} = \frac{(1+e_{\mathrm{T}})\,s}{\kappa_{\mathrm{s}}^{\mathrm{inter}}} \tag{44}$$

where $\kappa_{\mathrm{p}}^{\mathrm{inter}}$ is the elastic compression index in e^{inter}-ln$p$ plane and $\kappa_{\mathrm{s}}^{\mathrm{inter}}$ is the elastic parameter for the inter-grain pores in response to suction change.

Similar to the intra-grain micro-pores level, the plastic strain of inter-grain pores is produced due to SD or SI yielding ($\Delta\varepsilon^{p,SD,inter}$or $\Delta\varepsilon^{p,SI,inter}$) and LC yielding $\Delta\varepsilon^{p,LC,inter}$, as follows (Equation (45)):

$$\Delta\,\varepsilon^{p,inter} = \Delta\varepsilon^{p,SD,inter} + \Delta\varepsilon^{p,SI,inter} + \Delta\varepsilon^{p,LC,inter} \tag{45}$$

$\Delta\varepsilon^{p,SD,inter}$ or $\Delta\varepsilon^{p,SI,inter}$ is calculated by Equation (46) by considering the coupling function between intra-grain and inter-grain pores f_D^{inter} or f_I^{inter}:

$$\begin{aligned}\Delta\varepsilon^{p,SD,inter} &= f_D^{inter}\,\Delta\varepsilon_T^{intra}\\ \Delta\varepsilon^{p,SI,inter} &= f_I^{inter}\,\Delta\varepsilon_T^{intra}\end{aligned} \tag{46}$$

where f_D^{inter} and f_I^{inter} are the coupling functions between intra-grain pores and inter-grain pores in cases of suction decrease and suction increase, respectively. A common expression f^{inter} is used for f_D^{inter} and f_I^{inter}, as follows:

$$f^{inter} = \frac{a^{inter}}{1+\exp\left(b^{inter} + c^{inter}\frac{p}{p_0(s)}\right)} \tag{47}$$

where a^{inter}, b^{inter} and c^{inter} are parameters for f^{inter}. Different parameters are determined for f_D^{inter} and f_I^{inter}. $\Delta\varepsilon_T^{intra}$ is the incremental total strain for the intra-grain pores, expressed by Equation (48):

$$\Delta\,\varepsilon_T^{intra} = \Delta\varepsilon_m^{intra} + \Delta\varepsilon_M^{intra} \tag{48}$$

Since no water was found in inter-grain pores (see Figure 3), the suction effect is not considered. The incremental plastic volumetric strains for the intra-grain macro-pores due to LC yielding $\Delta\varepsilon^{p,LC,inter}$ is:

$$\Delta\,\varepsilon^{p,LC,inter} = -\frac{\lambda^{inter}(s)-\kappa_p^{inter}}{1+e_T}\frac{\Delta p_0}{p_0} \tag{49}$$

$p_0(s)$ can be determined by Equation (30). For suction-controlled oedometer tests, when the mean net stress (vertical stress) exceeds the pre-consolidation pressure and the suction is kept constant, $\Delta\varepsilon^{p,LC,inter}$ is:

$$\Delta\,\varepsilon_v^{p,LC,\,inter} = -\frac{\lambda^{inter}(s)-\kappa_p^{inter}}{1+e_T}\frac{\Delta p}{p} \tag{50}$$

The relationships between κ_{pm}^{intra}, κ_{pM}^{intra}, κ_p^{inter} and κ_T and between λ_m^{intra}, λ_M^{intra}, λ^{inter} and λ_T ought to satisfy the following Equations (51) and (52):

$$\kappa_T = \kappa_{pm}^{intra} + \kappa_{pM}^{intra} + \kappa_p^{inter} \tag{51}$$

$$\lambda_T\,(S) = \lambda_m^{intra}\,(s) + \lambda_M^{intra}(s) + \lambda^{inter}(s) \tag{52}$$

4 | DETERMINATION OF MODEL PARAMETERS

For the determination of parameters, the model was fitted to the results from suction-controlled oedometer tests conducted in this study. The model was then validated using the results of Molinero-Guerra et al.[22] who performed suction-controlled oedometer tests on MX80 bentonite pellet/powder mixture at a proportion of 80/20 in dry mass (80/20), together with the results of Darde[31] who performed swelling pressure tests on MX80 bentonite pellet/powder (70/30) mixture. The initial properties of the three tested mixtures (this study, Molinero-Guerra et al.[22] and Darde,[31] are presented in Table 2. The calculation of e_T of Darde[31] is presented in Appendix A.

TABLE 2 Properties of bentonite pellet/powder mixtures in three studies.

Property	This study	Molinero-Guerra et al.[22]	Darde[31]
7-mm Pellet:			
Dry density (Mg/m^3)	1.91	2.06	1.91
Void ratio, e_T^{intra}	0.44	0.34	0.45
Water content, w^{pellet} (%)	12.5	7.25	12
Suction (MPa)	87.4	132.4	89
Powder:			
Water content, w^{powder} (%)	5.66	3.17	3.5
Suction (MPa)	125.4	190.9	185
Mixture:			
Pellet/powder ratio	80/20	80/20	70/30
Diameter (mm)	50	50	60
Height (mm)	36	35	30
Dry density, p_d (Mg/m^3)	1.49	1.49	1.5015[c]
e_T	0.8376	0.8518	0.8448[c]
e^{inter}	0.3967	0.5118	0.3948
e_M^{intra}	0.04140	0.03376	0.04140[d]
e_m^{intra}	0.3995	0.3062	0.4086
Pressure/vertical stress (MPa)	0.1	0.1	0.004
Suction (MPa)	113	138	113
Test condition	Swell-consolidation[a]	Swell-consolidation[a]	Constant-volume[b]

[a]Suction-controlled high-pressure oedometer test.

[b]Swelling pressure test.

[c]With the help of the masses of pellets and powder grains (99.9 g and 39.5 g) and water contents, the initial dry density and initial void ratio of bentonite mixture of Darde[31] were re-calculated.

[d]The initial e_M^{intra} of this study was used instead, due to the lack of MIP results in Darde[31] for bentonite 7-mm pellet in initial state.

TABLE 3 Parameters of the water-retention model of this study by the PSO algorithm.

p_r	0.001	e_0	1.22				
S_{rm}^{intra}	α_p	α_s	m_1	m_2	m_3	m_4	m_5
	0.0024	0.048	0.60	1.60	144.96	1.04	0.06
S_r^{intra}	α_p	α_s	m_1	m_2	m_3	m_4	m_5
	0.0033	0.086	0.46	0.75	80.00	2.90	0.08
S_r	α_p	α_s	m_1	m_2	m_3	m_4	m_5
	0.011	0.091	0.55	0.76	4.00	2.39	0.35

4.1 | Hydraulic parameters

Zhang et al.[39] measured the void ratios and determined the water-retention properties of compacted MX80 bentonite which was instantaneously unloaded from oedometer cell. A suction increase, a tiny water loss and a limited rebounding were observed during the instantaneous unloading. The saturation degree measured after instantaneous unloading was close to that measured before unloading. The same procedure was applied in this study to determine the water retention properties of the studied mixture. Note that the same hydraulic parameters were used to model Molinero-Guerra et al.[22] and Darde[31] tests due to the lack of test data. The experimental values of S_{rm}^{intra}, S_r^{intra} and S_r were obtained from Equations (6), (8) and (9) and are presented in Figure 6, together with the fitting expression (Equation (10)). For the practical purpose, the imposed zero suction is presented as 0.1 MPa in a semi-log plot. An efficient artificial intelligence algorithm—Particle Swarm Optimization (PSO) method was employed in determining the parameters by matching the modelled results with the experimental ones.[41] The determined hydraulic parameters are presented in Table 3. It appears from Figure 6 that S_{rm}^{intra}, S_r^{intra} and S_r increased with the suction decrease and the stress increase. This suggests that the

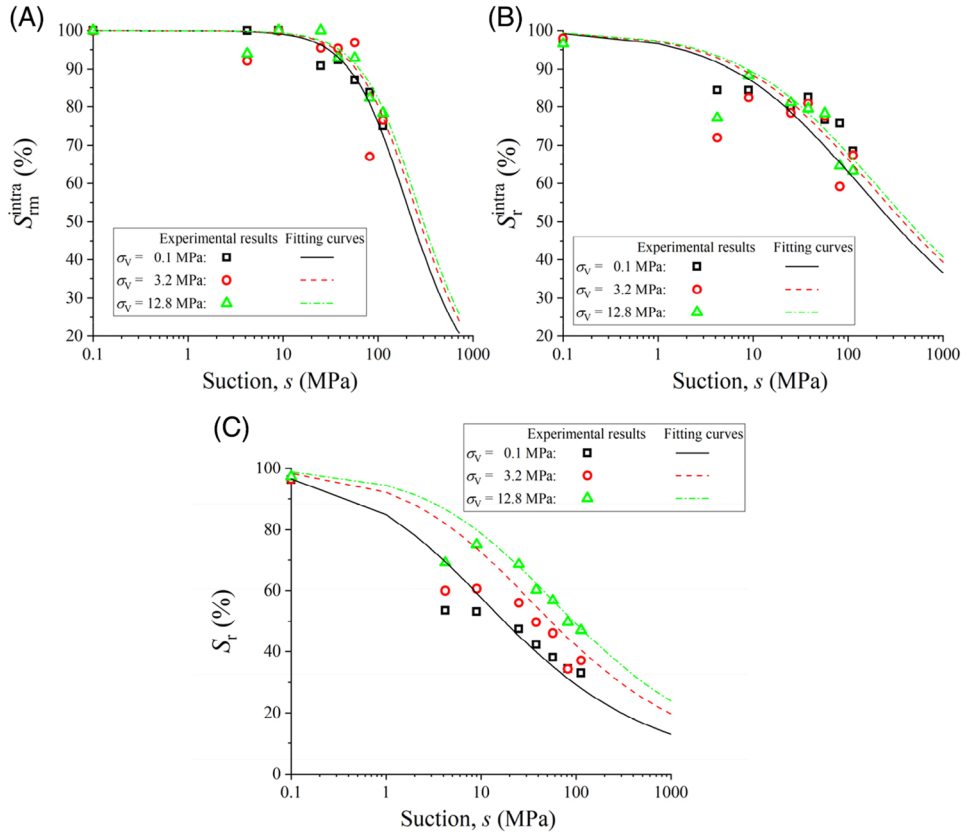

FIGURE 6 Soil-water characteristic curves for intra-grain micro-pores, total grain and total mixture (S_{rm}^{intra}, S_r^{intra} and S_r) of this study: (A) $S_{rm}^{intra} - s$; (B) $S_r^{intra} - s$; (C) $S_r - s$.

loading enhanced the water retention capacity. It was found that the fitting curves for S_{rm}^{intra}, S_r^{intra} and S_r matched well with the experimental results. Moreover, the S_r was close to 100% at zero suction, but was much smaller than 100% at $s \geq 4.2$ MPa. Considering that all the pores in the WC samples were filled by water due to the water injection technique, the S_r must be 100% before unloading. Therefore, the WC samples were categorized into the saturated samples, while the VET samples were classified into the unsaturated samples.

4.2 | Mechanical parameters

The compressibility parameters for the mixture are determined essentially based on suction-controlled oedometer tests in this study. The obtained parameters λ_T and κ_T are shown in Figure 7A. The large difference in λ_T between this study and Molinero-Guerra et al.[22] resulted from the different initial e_T^{intra} and e^{inter}. The λ_T of this study is fitted with Equation (53) in the form of BExM:

$$\lambda\ (s) = \lambda\,(0)\,[(1-r)\exp(\beta s) + r] \tag{53}$$

where r and β are parameters and $\lambda(0)$ is the saturated compressibility parameter. The parameters of λ_T of this study are presented in Table 4. The compressibility parameters at the levels of inter- and intra-grain pores λ_m^{intra}, λ_M^{intra} and λ^{inter} are determined using Equation (54):

$$\lambda = \frac{e_2 - e_1}{\ln(\sigma_2) - \ln(\sigma_1)} \tag{54}$$

where e_1 and e_2 refer to the void ratios of various pores (intra-grain micro- and macro-pores and inter-grain pores) at vertical stresses $\sigma_1 = 3.2$ MPa and $\sigma_2 = 12.8$ MPa. The calculated results are shown in Figure 7B. Note that if the calculated λ_M^{intra} at high suctions is smaller than zero due to cracking, λ_M^{intra} is taken as zero. It appears that λ_m^{intra}, λ_M^{intra} and λ^{inter} are

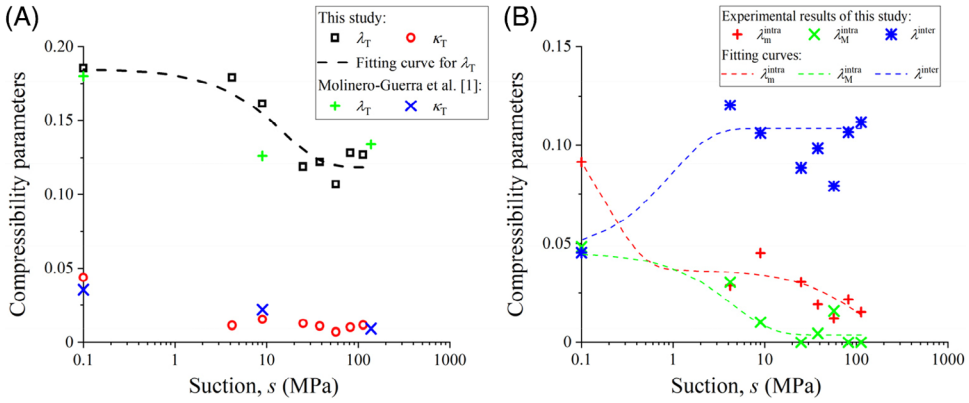

FIGURE 7 Compressibility parameters determined based on the tests in this study and in Molinero-Guerra et al.[22]: (A) λ_T and κ_T of this study and Molinero-Guerra et al.[22]; (B) λ_m^{intra}, λ_M^{intra}, λ^{inter} and λ_T of this study.

TABLE 4 Compressibility parameters.

Parameter	$\lambda(0)$	r	β	
λ_T of this study	0.185	0.64	−0.068	
λ_M^{intra} of this study	0.048	0.0012	−0.014	
λ^{inter} of this study	0.046	2.38	−1.05	
λ^{inter} of Molinero-Guerra et al.[22]	0.05	2.78	−0.10	
$\lambda^{inter}(s)$ of Darde[31]	0.087	2.15	−0.26	
$\lambda_m^{intra}(s)$ of this study	a	b	c	d
	0.097	−5.66	0.037	−0.009

highly suction dependent. Only λ_m^{intra} is fitted with Equation (55), whereas λ_M^{intra} and λ^{inter} are still fitted with Equation (53).

$$\lambda_m^{intra}(s) = a\exp(bs) + c\exp(ds) \tag{55}$$

where a, b, c and d are parameters. All compressibility parameters are summarized in Table 4.

Due to the difference in e^{inter} between the three studies and the important role played by inter-grain pores in the global volume change behaviour of the whole mixture, λ^{inter} of Molinero-Guerra et al.[22] and Darde[31] should be different to those of this study. The parameters from the tests in this study and from the tests in Molinero-Guerra et al.[22] and Darde[31] are also summarised in Table 4.

The saturated pre-consolidation pressure of bentonite pellet/powder mixture of this study (1.32 MPa) is taken as the value for p_0^*. The other parameters of this triple-microstructure constitutive damage model are determined with the PSO algorithm by matching the modelled compression curves with the experimental results shown in Figure 10A. Note that κ_{pm}^{intra}, κ_{pM}^{intra} and κ_p^{inter} of the unsaturated (VET) samples and the saturated (WC) samples are determined separately, since the κ_T values of the saturated samples are markedly higher than that of the unsaturated samples. All the parameters are summarised in Table 5.

Due to the different initial conditions, some parameters of Molinero-Guerra et al.[22] and Darde[31] (Tables 6 and 7) are adjusted by matching the modelled results with the experimental ones by the PSO algorithm (Figure 8). The fitting curves for pre-consolidation pressure of this study matched with the experimental results (Figure 9).

5 | TEST SIMULATIONS AND DISCUSSIONS

As mentioned previously, the model results are firstly fitted to the oedometer tests of this study. Then, the results of Molinero-Guerra et al.[22] and Darde[31] are used to validate the proposed model.

TABLE 5 Parameters of this study by the PSO algorithm.

κ_{sm}^{intra}	κ_{sM}^{intra}	κ_{s}^{inter}	κ_{pm}^{intra*}	κ_{pM}^{intra*}
0.048	0.038	0.0048	0.0024/0.031*	0.00088/0.0038*
κ_{p}^{inter*}	$h_{s,imi}$	h_1	h_2	$h_{s,ima}$
0.0079/0.0083*	2.54×10^{-5}	5.14	3.10	3.31×10^{-4}
h_3	h_4	a_M^{intra}	b_M^{intra}	c_M^{intra}
0.10	6.93	64.37	15.68	11.44
a^{inter}	b^{inter}	c^{inter}	α_m^{intra}	α_M^{intra}
−0.28	9.74	−175.10	1.13	3.53
p_0^*	p_c			
1.32	0.87			

*The left was for the unsaturated samples and the right was for the saturated (WC) samples. Taking κ_{pm}^{intra} as an example, 0.0024 was for the unsaturated (VET) samples and 0.031 was for the saturated (WC) samples.

TABLE 6 Adjusted parameters of Molinero-Guerra et al.[22] by the PSO algorithm.

κ_{sm}^{intra}	κ_{sM}^{intra}	κ_{s}^{inter}	κ_{pM}^{intra*}
0.057	0.020	0.010	0.0013*
κ_{p}^{inter*}	a^{inter}	b^{inter}	c^{inter-}
0.0040*	−0.70	131.14	−1546.29

*Only κ_{pM}^{intra} and κ_{p}^{inter} of the saturated samples are adjusted, while those of the unsaturated samples are kept the same as the parameters from the results of this study.

TABLE 7 Adjusted parameters of Darde[31] by the PSO algorithm.

κ_{s}^{inter}	a^{inter}	c^{inter}
0.018	−0.40	−400.10

5.1 | Wetting-induced swelling and compression behaviour

The model results from the suction-controlled oedometer tests of this study and Molinero-Guerra et al.[22] are presented in Figures 10 and 11, respectively. It appears from Figures 10A and 11 that for the two studies, the model results agree well with the experimental ones in terms of wetting-induced swelling and loading-induced compression for the bentonite mixture. The unloading behaviour of the mixture in Molinero-Guerra et al.[22] is also well reproduced.

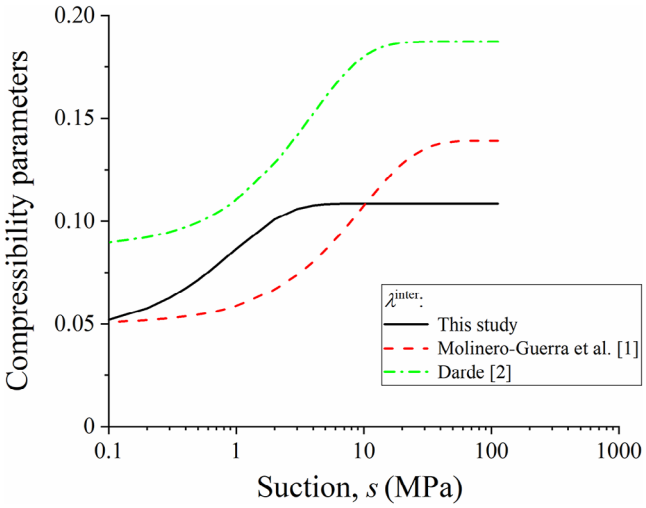

FIGURE 8 Fitting curves of λ^{inter} of this study, Molinero-Guerra et al.[1] and Darde.[2]

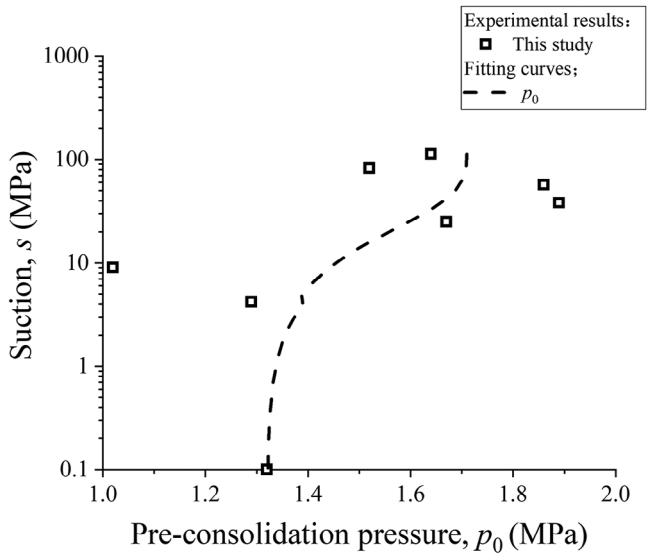

FIGURE 9 Fitting curves for pre-consolidation pressures of this study (loading-collapse LC curve).

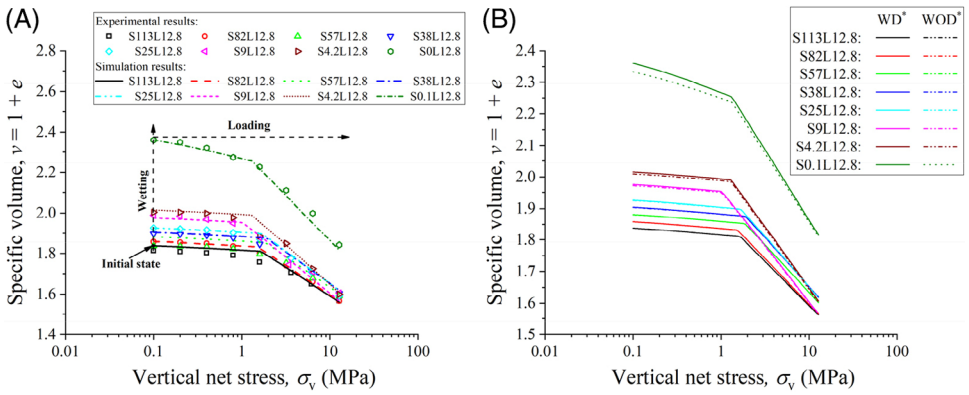

FIGURE 10 Modelling suction-controlled high-pressure oedometer tests of this study on MX80 bentonite pellet/powder (80/20) mixture: (A) modelling with damage model; (B) comparison of modelling with and without consideration of damage (*WD: modelling with damage; WOD: modelling without damage).

The model results with and without consideration of damage for the two studies are compared in Figures 10B and 11. For the wetting stage, the damage effect is found identifiable at low suctions ($s \leq 9$ MPa), but insignificant at high suctions ($s \geq 25$ MPa). Conversely, the damage effect appears negligible in the loadings stage, because intra-grain macro-pores are related to damage and the loading reduce the intra-grain macro-pore value thus the damage.

5.2 | Microstructure evolution upon loading

The evolutions of the three pore structures of bentonite pellet/powder mixture of this study under oedometer loading at constant suction are modelled and are depicted in Figure 12. The experimental results are extracted from Figure 4. Three samples 'S113L0.1', 'S113L3.2' and 'S113L12.8' are presented in Figure 12A. It was worth noting that the experimental e_m^{intra}, e_M^{intra}, e^{inter} and e_T at initial state were determined from sample 'S113L0.1' instead of 'S113L12.8', leading to the difference between model results and experimental ones of 'S113L12.8' (Figure 12A). It appears from Figure 12 that, for all suctions, the modelled e_m^{intra}, e_M^{intra}, e^{inter} and e_T match well with the experimental ones, except for e_M^{intra} at high suctions 113, 82 and 57 MPa, possibly because without considering the deviatoric deformation of pellets at hight suctions, the volume increase in intra-grain macro-pores due to cracking cannot be taken into account.

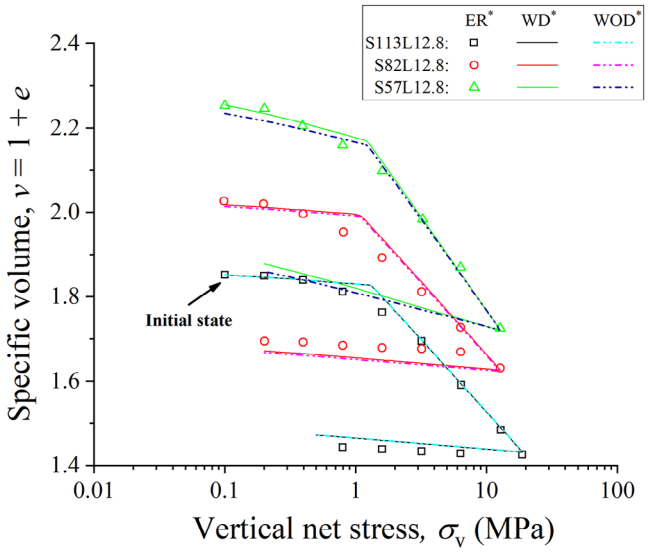

FIGURE 11 Modelling suction-controlled high-pressure oedometer tests of Molinero-Guerra et al.[22] on MX80 bentonite pellet/powder (80/20) mixture (*ER: experimental results; WD: modelling with consideration of damage; WOD: modelling without consideration of damage).

The evolutions of the three pore structures under loading at constant suction of Molinero-Guerra et al.[22] are depicted in Figure 13. Note that in both cases (Figures 12 and 13), for the unsaturated samples ($s \geq 4.2$ MPa), the variations of $e_{\mathrm{m}}^{\mathrm{intra}}$, $e_{\mathrm{M}}^{\mathrm{intra}}$, e^{inter} and e_{T} are negligible before reaching the pre-consolidation pressure. Beyond the pre-consolidation pressure, the decrease in e^{inter} becomes significant, contributing to a large variation of e_{T}. In addition, the decrease in $e_{\mathrm{m}}^{\mathrm{intra}}$ gradually becomes larger with the suction decrease to 4.2 MPa. On the contrary, the decrease in $e_{\mathrm{m}}^{\mathrm{intra}}$ for the saturated samples (zero suction) in the two studies was significant due to the low stiffness of grains at such suction, which makes the variation of e_{T} predominant from the beginning of loading. When the pre-consolidation pressure is exceeded, the decreases in $e_{\mathrm{M}}^{\mathrm{intra}}$ and e^{inter} can be observed from Figure 13 and are close to each other. Summarising, the global compression behaviour of mixture samples is governed by the filling of inter-grain pores for the unsaturated samples, but by the grain compression for the saturated samples.

5.3 | Swelling pressure and water content evolutions upon wetting

The development of swelling pressure upon wetting is modelled by applying the back compaction method.[40] The computation of swelling pressure can be performed in two stages at a certain suction and stress state: (1) to calculate the swelling strain of various pores by allowing swelling in the first stage; (2) to compress the produced swelling strain back and calculate the resulting stress after the compression process. The modelling was carried out with the suction decreased to 0.1 MPa at constant volume conditions. Note that only the elastic strain was induced by loading when the stress was smaller than the pre-consolidation pressure, whereas the elasto-plastic strain was induced by loading when the stress exceeded the pre-consolidation pressure. Thereby, the predicted swelling pressure can be obtained. The initial properties of the bentonite mixture in the swelling pressure test of Darde[31] are summarized in Table 1. The model results of swelling pressure P_{s} evolution upon wetting under constant volume condition is presented in Figure 14, together with experimental results. It appears that the modelled P_{s} agrees well with the experimental results, except for the P_{s} at high suctions ($s \geq 10$ MPa). This large difference results from the consideration of only the elastic strain induced by loading when the stress was smaller than the pre-consolidation pressure. The sharp increase of the modelled P_{s} is induced by the development of elastoplastic strain hardening. It is also observed that the modelled P_{s} without consideration of damage is clearly lower than the experimental one, indicating the important effect of damage.

The evolution of water content with suction at the intra grain level is analysed and the results are shown in Figure 15. For simplicity, the saturated water content of intra-grain micro-pores $w_{\mathrm{msa}}^{\mathrm{intra}}$ is calculated by assuming the intra-grain micro-pores saturated. The intersection of $w_{\mathrm{msa}}^{\mathrm{intra}}$ and the water content of whole mixture w^{mixture} indicates that water saturates the intra-grain micro-pores at suction 19 MPa, and then starts filling the intra-grain macro-pores. When reaching suction

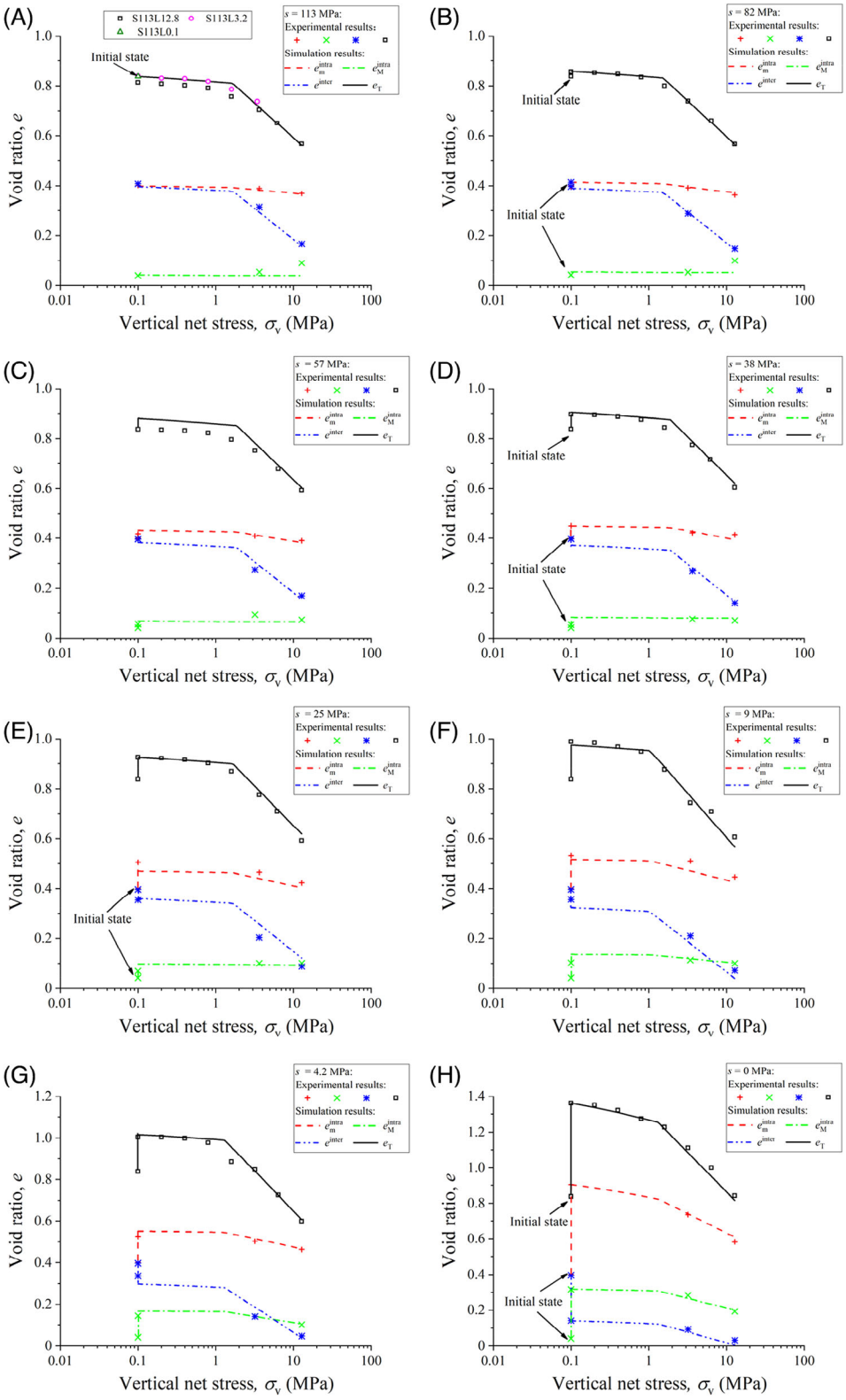

FIGURE 12 Evolutions of the three pore structures of MX80 bentonite pellet/powder (80/20) mixture under oedometer loading at constant suction in this study: (A) s = 113MPa; (B) s = 82 MPa; (C) s = 57 MPa; (D) s = 38 MPa; (E) s = 25 MPa; (F) s = 9 MPa; (G) s = 4.2 MPa; (H) s = 0 MPa.

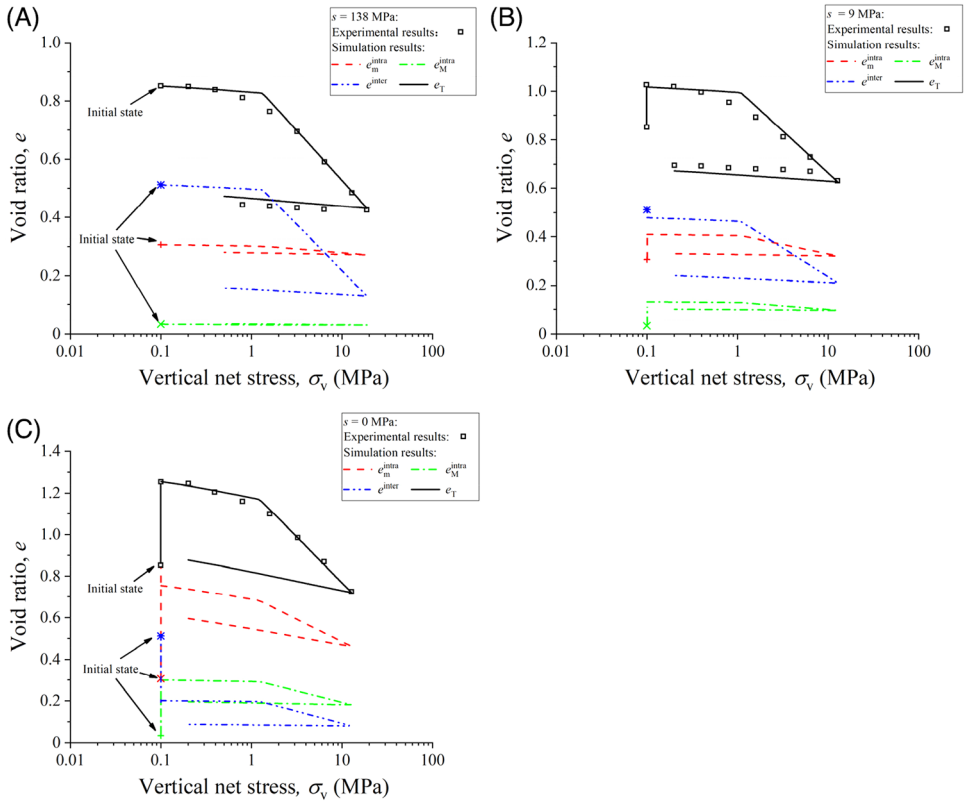

FIGURE 13 Evolutions of three pore structures of MX80 bentonite pellet/powder (80/20) mixture under oedometer loading at constant suction in Molinero-Guerra et al.[22]: (A) $s = 138$ MPa; (B) $s = 9$ MPa; (C) $s = 0$ MPa.

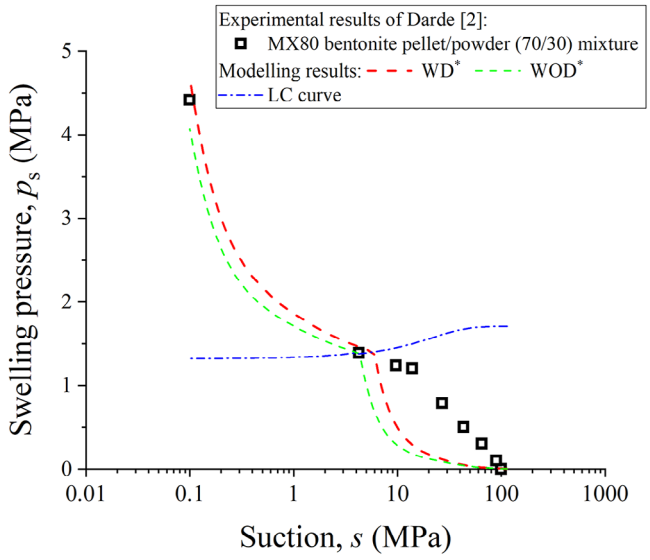

FIGURE 14 Modelling the swelling pressure test of Darde[31] on MX80 bentonite pellet/powder (70/30) mixture upon wetting under constant volume condition (*WD: with consideration of damage; WOD: without consideration of damage).

0.1 MPa, the inter-grain pores and intra-grain macro-pores are closed, leading water to come back to intra-grain micro-pores. Similar observation was reported by Wang et al.[40] on the water-retention results of MX80 bentonite/sand mixture upon wetting under constant volume condition. The difference in the w^{mixture} between the model results with and without consideration of damage model appears smaller than that for $w^{\text{intra}}_{\text{msa}}$.

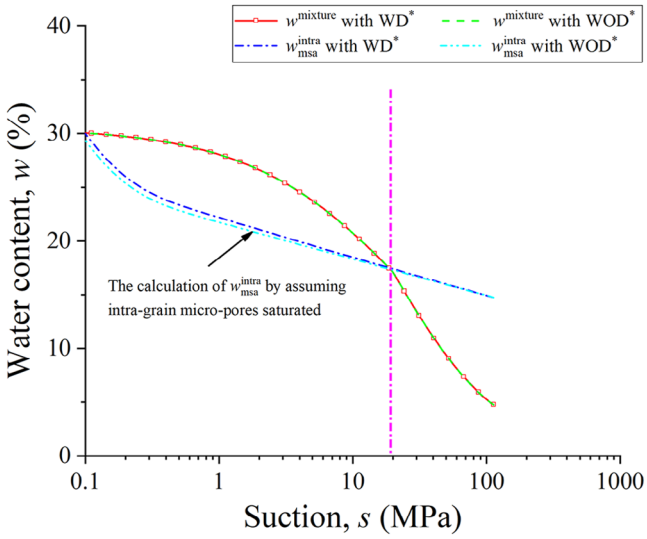

FIGURE 15 Water content of MX80 bentonite pellet/powder (70/30) mixture upon wetting under constant volume: (*WD: with consideration of damage; WOD: without consideration of damage).

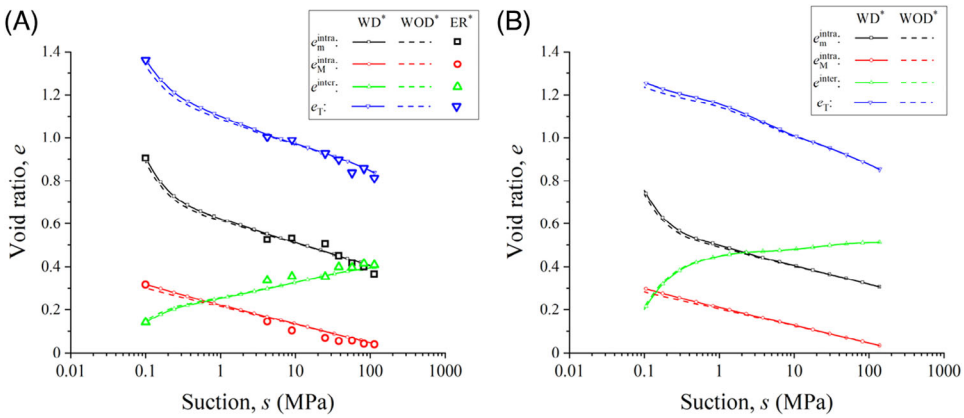

FIGURE 16 Modelling the evolutions of the three pore structures of MX80 bentonite pellet/powder (80/20) mixture upon wetting under a vertical stress of 0.1 MPa: (A) this study; (B) Molinero-Guerra et al.[22] (*ER: experimental results; *WD: modelling with consideration of damage; WOD: modelling without consideration of damage).

5.4 | Microstructure evolution upon wetting

The evolutions of the three pores structures of MX80 bentonite pellet/powder (80/20) mixture upon wetting under a vertical stress of 0.1 MPa in this study and in Molinero-Guerra et al.[22] are presented in Figure 16A,B, respectively. The experimental results are extracted from Figure 4. Figure 16A shows that e_m^{intra}, e_M^{intra} and e_T consistently increase with the suction decrease, while e^{inter} continuously decreases, indicating the filling of inter-grain pores due to the swelling of pellets and powder grains. The variation of e_T is governed by e_m^{intra}. As observed from Figure 16B, e_m^{intra}, e_M^{intra} and e_T also consistently increase with the suction decrease, while e^{inter} is decreasing. The decreasing rate of e^{inter} is suddenly accelerated when the suction is smaller than 0.9 MPa, indicating a rapid filling of inter-grain pores upon further wetting. This results from the disaggregation of pellets and powder grains due to liquid water injection.[7,22,42] Moreover, the increasing rate of e_T slows down because of the suddenly accelerated filling of inter-grain pores.

The evolutions of the three pore structures of MX80 bentonite pellet/powder (70/30) mixture upon wetting under constant-volume condition of Darde[31] are presented in Figure 17, with e_T keeping constant. When the suction decreases from 113 to around 0.9 MPa, the e_m^{intra} and e_M^{intra} increase together with the e^{inter} which decreases to zero, indicating the filling of inter-grain pores due to the swelling of pellets and powder grains. Upon further wetting to suction 0.1 MPa, the e_M^{intra} nearly decreases to zero, which indicates that the intra-grain macro-pores are highly closed. In addition, the

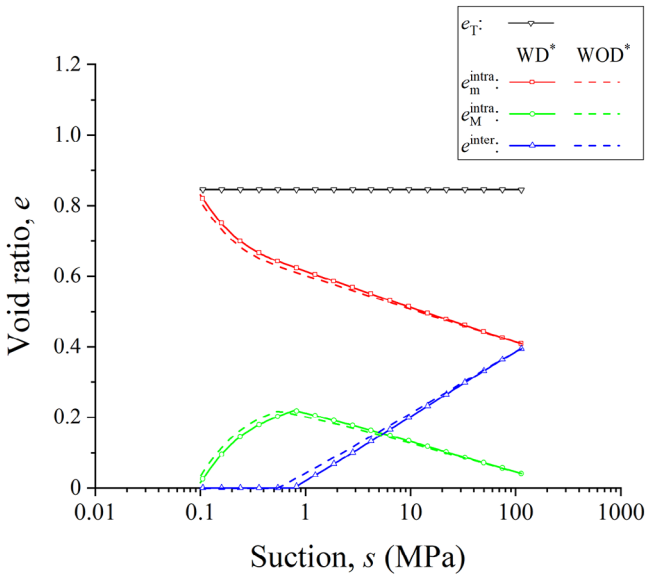

FIGURE 17 Modelling the evolutions of the three pore structures of MX80 bentonite pellet/powder (70/30) mixture upon wetting under constant volume of Darde[31] (*WD: with consideration of damage; WOD: without consideration of damage).

microstructure evolutions with and without consideration of damage model appears smaller than that for P_s, indicating that P_s is more sensitive to the damage than the microstructure evolutions.

6 | CONCLUSIONS

In this study, a triple-microstructure hydro-mechanical constitutive damage model was proposed to describe the hydro-mechanical behaviour of MX80 bentonite pellet/powder mixture. A series of suction-controlled oedometer tests were performed on the bentonite mixture. The microstructural characteristics of the pellet/powder mixture were analysed, providing a rich hydro-mechanical data base for the model development. In particular, the pellet damage due to both wetting and loading was identified and modelled. The model parameters were determined essentially based on the laboratory tests performed in this study. The model response was firstly verified with the test results of this study. Then, the results of Molinero-Guerra et al.[22] and Darde[31] who respectively carried out suction-controlled oedometer tests and swelling pressure tests on the same bentonite pellet/powder mixture were employed to validate the proposed model.

The volume change behaviour and the development of swelling pressure can be well described by the model. The evolutions of the three pore structures of bentonite pellet/powder mixture were also well depicted. It appears that under suction-controlled oedometer loading condition, the global compression behaviour was governed by the filling of inter-grain pores for the unsaturated samples, but by the compression of grains for the saturated samples. Conversely, when wetted under constant-volume condition, the inter-grain pores and intra-grain macro-pores were closed, due to the swelling of intra-grain micro-pores. The water-retention results showed that water saturated the intra-grain micro-pores at suction 19 MPa, and then started filling the intra-grain macro-pores. When the inter-grain pores and the intra-grain macro-pores were all closed at suction 0.1 MPa, water came back to the intra-grain micro-pores.

Under suction-controlled oedometer loading, the damage effect was found to be significant during wetting to a low suction, contrary to the insignificant damage effect during loading, the loading reduced the intra-grain macro-pore value thus the damage. When wetting under constant-volume condition, it appears that the damage affected the swelling pressure and the microstructure evolutions.

On the whole, the main features of the hydro-mechanical behaviour of MX80 bentonite pellet/powder mixture could be well described by the proposed triple-microstructure hydro-mechanical constitutive damage model.

Notation

$\Delta\varepsilon_M^{e,intra}$ elastic incremental strain for intra-grain macro-pores
$\Delta\varepsilon_M^{p,intra}$ plastic incremental strain for intra-grain macro-pores

$\Delta\varepsilon_{\mathrm{M}}^{\mathrm{p,SD,intra}}$	plastic incremental strain for intra-grain macro-pores induced by SD yielding
$\Delta\varepsilon_{\mathrm{m}}^{\mathrm{e,intra}}$	elastic incremental strain for intra-grain micro-pores
$\Delta\varepsilon_{\mathrm{m}}^{\mathrm{intra}}$	total incremental strain for intra-grain micro-pores
$\Delta\varepsilon_{\mathrm{M}}^{\mathrm{intra}}$	total incremental strain for intra-grain macro-pores
$\Delta\varepsilon_{m}^{\mathrm{p,intra}}$	plastic incremental strain for intra-grain micro-pores
$h_{\mathrm{LC,ima}}$	parameter that controls the softening or hardening of the LC curve due to SD or SI yielding for intra-grain macro-pores
$h_{\mathrm{LC,imi}}$	parameter that controls the softening or hardening of the LC curve due to SD or SI yielding for intra-grain micro-pores
$h_{\mathrm{s,ima}}$	parameter that controls the inward movement of SD yield curve or outward movement of SI yield curve for intra-grain macro-pores
$h_{\mathrm{s,imi}}$	parameter that controls the inward movement of SD yield curve or outward movement of SI yield curve for intra-grain micro-pores
$K_{\mathrm{p}}^{\mathrm{inter}}$	bulk modulus for inter-grain pores for stress
$K_{\mathrm{pm}}^{\mathrm{intra}}$	bulk modulus for intra-grain micro-pores for stress
$K_{\mathrm{pM}}^{\mathrm{intra}}$	bulk modulus for intra-grain macro-pores for stress
$K_{\mathrm{s}}^{\mathrm{inter}}$	bulk modulus for inter-grain pores for suction
$K_{\mathrm{sm}}^{\mathrm{intra}}$	bulk modulus for intra-grain micro-pores for suction
$K_{\mathrm{sM}}^{\mathrm{intra}}$	bulk modulus for intra-grain macro-pores for suction
S_{r}	saturation degree of whole mixture
$S_{\mathrm{r}}^{\mathrm{intra}}$	saturation degree of whole grain
$S_{\mathrm{rm}}^{\mathrm{intra}}$	saturation degree of intra-grain micro-pores
$S_{\mathrm{rM}}^{\mathrm{intra}}$	saturation degree of intra-grain macro-pores
V^{inter}	volume of inter-grain pores
$V_{\mathrm{m}}^{\mathrm{intra}}$	volume of intra-grain micro-pores
$V_{\mathrm{M}}^{\mathrm{intra}}$	volume of intra-grain macro-pores
V_{s}	solid volume
$V_{\mathrm{V,wm}}^{\mathrm{intra}}$	volume of water stored in intra-grain micro-pores
$V_{\mathrm{V,wM}}^{\mathrm{intra}}$	volume of water stored in intra-grain macro-pores
e^{inter}	void ratio of inter-grain pores
$e_{\mathrm{m}}^{\mathrm{intra}}$	void ratio of intra-grain micro-pores
$e_{\mathrm{M}}^{\mathrm{intra}}$	void ratio of intra-grain macro-pores
e_{T}	total void ratio of mixture
$e_{\mathrm{T}}^{\mathrm{intra}}$	total void ratio of grain
$e_{\mathrm{wm}}^{\mathrm{intra}}$	water void ratio of intra-grain micro-pores
$e_{\mathrm{wM}}^{\mathrm{intra}}$	water void ratio of intra-grain macro-pores
$f_{\mathrm{D}}^{\mathrm{inter}}$	coupling function between intra-grain pores and inter-grain pores in case of suction decrease
$f_{\mathrm{I}}^{\mathrm{inter}}$	coupling function between intra-grain pores and inter-grain pores in case of suction increase
$f_{\mathrm{MD}}^{\mathrm{intra}}$	coupling function between intra-grain micro- and macro-pores in case of suction decrease
$f_{\mathrm{MI}}^{\mathrm{intra}}$	coupling function between intra-grain micro- and macro-pores in case of suction increase
p_0^*	saturated pre-consolidation pressure of mixture
$p_0(s)$	pre-consolidation pressure of mixture at a given suction
p_{c}	reference pressure for mixture
p_{d}	dry density
w^{mixture}	water content of whole mixture
$w_{\mathrm{msa}}^{\mathrm{intra}}$	saturated water content of intra-grain micro-pores
$\alpha_{\mathrm{m}}^{\mathrm{intra}}$	power parameter related to $S_{\mathrm{rm}}^{\mathrm{intra}}$
$\alpha_{\mathrm{M}}^{\mathrm{intra}}$	power parameter related to $S_{\mathrm{rM}}^{\mathrm{intra}}$
$\varepsilon^{\mathrm{inter}}$	volumetric strain of inter-grain pores
$\varepsilon_{\mathrm{m}}^{\mathrm{intra}}$	volumetric strain of intra-grain micro-pores
$\varepsilon_{\mathrm{M}}^{\mathrm{intra}}$	volumetric strain of intra-grain macro-pores

ε_T	total volumetric strain
κ_p^{inter}	elastic compression index in e^{inter}-ln$p$ plane
κ_{pm}^{intra}	elastic compression index in e_m^{intra}-ln$p$ plane
κ_{pM}^{intra}	elastic compression index in e_M^{intra}-ln$p$ plane
κ_s^{inter}	elastic parameter for inter-grain pores with suction changes
κ_{sm}^{intra}	elastic parameter for intra-grain micro-pores with suction changes
κ_{sM}^{intra}	elastic parameter for intra-grain macro-pores with suction changes
κ_T	elastic compression index in e_T-ln$p$ plane
$\lambda^{inter}(s)$	slope of the virgin consolidation line in e^{inter}-ln$p$ plane at a given suction s
$\lambda_m^{intra}(s)$	slope of the virgin consolidation line in e_m^{intra}-ln$p$ plane at a given suction s
$\lambda_M^{intra}(s)$	slope of the virgin consolidation line in e_M^{intra}-ln$p$ plane at a given suction s
$\lambda_T(s)$	slope of the virgin consolidation line in e_T-ln$p$ plane at a given suction s
$\Delta\varepsilon^{e,inter}$	elastic incremental strain for inter-grain pores
$\Delta\varepsilon^{inter}$	total incremental strain for inter-grain pores
$\Delta\varepsilon_M^{p,LC,intra}$	plastic incremental strain for intra-grain macro-pores induced by LC yielding
$\Delta\varepsilon_M^{p,SI,intra}$	plastic incremental strain for intra-grain macro-pores induced by SI yielding
$\Delta\varepsilon^{p,inter}$	plastic incremental strain for inter-grain pores
$\Delta\varepsilon^{p,LC,inter}$	plastic incremental strain for inter-grain pores induced by LC yielding
$\Delta\varepsilon^{p,SD,inter}$	plastic incremental strain for inter-grain pores induced by SD yielding
$\Delta\varepsilon^{p,SI,inter}$	plastic incremental strain for inter-grain pores induced by SI yielding
$\Delta\varepsilon_T^{intra}$	total incremental strain for the intra-grain pores
D	damage coefficient
$D_{L0.1}$	damage coefficient at a given suction under initial load
$D_{S113L0.1}$	damage coefficient at initial state
m^{pellet}	initial mass of pellets
m^{powder}	initial mass of powder grains
m_s	total mass of pellets and powder grains in dry mass
p	mean net stress
P_s	swelling pressure
p_s	density of soil particles
s	suction
w^{pellet}	water content of pellets
w^{powder}	water content of powder grains
$\Delta D^{loading}$	change in loading-induced damage
$\Delta D^{wetting}$	change in wetting-induced damage

ACKNOWLEDGEMENTS

The authors would like to thank the China Scholarship Council (CSC). The supports provided by Ecole des Ponts ParisTech (ENPC) and Institut de Radioprotection et de SÛreté Nucléaire (IRSN) are also greatly acknowledged.

CONFLICT OF INTEREST STATEMENT

The authors declare no conflicts of interest.

DATA AVAILABILITY STATEMENT

Data will be available from the authors upon reasonable request.

ORCID

Jin-Wen Yang https://orcid.org/0000-0002-0541-1402
Hao Wang https://orcid.org/0000-0003-1829-1013

REFERENCES

1. Pusch R. Highly compacted sodium bentonite for isolating rock-deposited radioactive waste products. *Nucl Technol*. 1979;45:153-157. doi:10.13182/NT79-A32305
2. Alonso EE, Romero E, Hoffmann C, García-Escudero E. Expansive bentonite-sand mixtures in cyclic controlled-suction drying and wetting. *Eng Geol*. 2005;81:213-226. doi:10.1016/j.enggeo.2005.06.009
3. Gens A. Soil-environment interactions in geotechnical engineering. *Geotechnique*. 2010;60:3-74. doi:10.1680/geot.9.P.109
4. Cui YJ, Tang AM, Qian LX, Ye WM, Chen B. Thermal-mechanical behavior of compacted GMZ bentonite. *Soils Found*. 2011;51:1065-1074. doi:10.3208/sandf.51.1065
5. Mokni N, Molinero-Guerra A, Cui YJ, et al. Modelling the long-term hydro-mechanical behaviour of a bentonite pellet/powder mixture with consideration of initial structural heterogeneities. *Geotechnique*. 2020;70:563-580. doi:10.1680/jgeot.18.P.110
6. Zeng Z. Investigation of the hydro-mechanical behaviour of compacted bentonite/claystone mixture. Ecole des Ponts Paristech; 2021.
7. Zhang Z, Cui Y, Yang J, Mokni N. Investigation into the hydro-mechanical behaviour and microstructural evolution of MX80 bentonite pellet upon wetting/drying. *Constr Build Mater*. 2022;345:1-12.
8. Gens A, Alonso EE. A framework for behavior of unsaturated expansive clay.pdf. *Can Geotech J*. 1992;29:1013-1032.
9. Alonso EE, Vaunat J, Gens A. Modelling the mechanical behaviour of expansive clays. *Eng Geol*. 1999;54:173-183.
10. Qiao Y, Ding W, Laloui L. Constitutive framework for unsaturated soils with differentiation of capillarity and adsorption. *Springer Ser Geomech Geoengin*. 2017;2:447-454. doi:10.1007/978-3-319-52773-4_53
11. Takayama Y, Tachibana S, Iizuka A, Kawai K, Kobayashi I. Constitutive modeling for compacted bentonite buffer materials as unsaturated and saturated porous media. *Soils Found*. 2017;57:80-91. doi:10.1016/j.sandf.2017.01.006
12. Guo G, Fall M. Modelling of dilatancy-controlled gas flow in saturated bentonite with double porosity and double effective stress concepts. *Eng Geol*. 2018;243:253-271. doi:10.1016/j.enggeo.2018.07.002
13. Qiao Y, Xiao Y, Laloui L, Ding W, He M. A double-structure hydromechanical constitutive model for compacted bentonite. *Comput Geotech*. 2019;115:103173. doi:10.1016/j.compgeo.2019.103173
14. Zeng Z, Cui YJ, Zhang F, Conil N, Talandier J. Investigation of swelling pressure of bentonite/claystone mixture in the full range of bentonite fraction. *Appl Clay Sci*. 2019;178:105137. doi:10.1016/j.clay.2019.105137
15. Musso G, Azizi A, Jommi C. A microstructure-based elastoplastic model to describe the behaviour of a compacted clayey silt in isotropic and triaxial compression. *Can Geotech J*. 2020;57:1025-1043. doi:10.1139/cgj-2019-0176
16. Navarro V, Asensio L, Gharbieh H, De la Morena G, Pulkkanen VM. A triple porosity hydro-mechanical model for MX-80 bentonite pellet mixtures. *Eng Geol*. 2020;265:105311. doi:10.1016/j.enggeo.2019.105311
17. Navarro V, Cabrera V, De la Morena G, Asensio L, Yustres Á, Torres-Serra J. A new double-porosity macroscopic model of bentonite free swelling. *Eng Geol*. 2022;305:106725. doi:10.1016/j.enggeo.2022.106725
18. Gens A, Sánchez M, Sheng D. On constitutive modelling of unsaturated soils. *Acta Geotech*. 2006;1:137-147. doi:10.1007/s11440-006-0013-9
19. Cardoso R, Alonso EE, Maranha Das Neves E. A constitutive model for compacted expansive and bonded marls. *Geotechnique*. 2013;63:1116-1130. doi:10.1680/geot.12.P.101
20. Mašín D. Double structure hydromechanical coupling formalism and a model for unsaturated expansive clays. *Eng Geol*. 2013;165:73-88. doi:10.1016/j.enggeo.2013.05.026
21. Wheeler SJ, Sharma RS, Buisson MSR. Coupling of hydraulic hysteresis and stress-strain behaviour in unsaturated soils. *Geotechnique*. 2003;53:41-54. doi:10.1680/geot.2003.53.1.41
22. Molinero-Guerra A, Cui YJ, He Y, et al. Characterization of water retention, compressibility and swelling properties of a pellet/powder bentonite mixture. *Eng Geol*. 2019;248:14-21. doi:10.1016/j.enggeo.2018.11.005
23. Hoffmann C, Alonso EE, Romero E. Hydro-mechanical behaviour of bentonite pellet mixtures. *Phys Chem Earth*. 2007;32:832-849. doi:10.1016/j.pce.2006.04.037
24. Alonso EE, Romero E, Hoffmann C. Hydromechanical behaviour of compacted granular expansive mixtures: experimental and constitutive study. *Geotechnique*. 2011;61:329-344. doi:10.1680/geot.2011.61.4.329
25. Molinero-Guerra A, Delage P, Cui YJ, et al. Water-retention properties and microstructure changes of a bentonite pellet upon wetting/drying; application to radioactive waste disposal. *Geotechnique*. 2020;70:199-209. doi:10.1680/jgeot.17.P.291
26. Zhang Z. Investigation on volume change behavior of GMZ bentonite pellet mixtures under hydro- mechanical coupling condition. Tongji University; 2021.
27. Navarro V, Asensio L, De la Morena G, Gharbieh H, Alonso J, Pulkkanen VM. From double to triple porosity modelling of bentonite pellet mixtures. *Eng Geol*. 2020;274:105714. doi:10.1016/j.enggeo.2020.105714
28. Molinero-Guerra A, Aimedieu P, Bornert M, et al. Analysis of the structural changes of a pellet/powder bentonite mixture upon wetting by X-ray computed microtomography. *Appl Clay Sci*. 2018;165:164-169. doi:10.1016/j.clay.2018.07.043
29. Molinero-Guerra A, Cui YJ, Mokni N, et al. Investigation of the hydro-mechanical behaviour of a pellet/powder MX80 bentonite mixture using an infiltration column. *Eng Geol*. 2018;243:18-25. doi:10.1016/j.enggeo.2018.06.006
30. Molinero-Guerra A. Experimental and Numerical Characterizations of the Hydro-Mechanical Behavior of a Heterogeneous Material: Pellet/Powder Bentonite Mixture. Ecole des Ponts Paristech; 2019.
31. Darde B. Experimental and Numerical Study of the Hydromechanical Behaviour of Bentonite Pellet-Powder Mixtures. Ecole des Ponts Paristech; 2020.

32. Saba S. Hydro-Mechanical Behaviour of Bentonite-Sand Mixture Used As Sealing Materials In Radioactive Waste Disposal Galleries. Ecole des Ponts Paristech; 2013.
33. Wang Q, Cui YJ, Tang AM, Li XL, Ye WM. Time- and density-dependent microstructure features of compacted bentonite. *Soils Found*. 2014;54:657-666. doi:10.1016/j.sandf.2014.06.021
34. Webb PA. Volume and Density Determinations for Particle Technologists. *Micromeritics Instrument Corporation*. 2001;1-16.
35. Su Y, Cui Y-J, Dupla J-C, Canou J, Qi S. Developing a sample preparation approach to study the mechanical behavior of unsaturated fine/coarse soil mixture. *Geotech Test J*. 2021;44:20190450. doi:10.1520/GTJ20190450
36. Yang J-W, Cui Y, Mokni N, Ormea E. Investigation into the mercury intrusion porosimetry (MIP) and micro- computed tomography (μCT) methods for determining the pore size distribution of MX80 bentonite pellet. *Acta Geotech*. 2023:1-13.
37. Wang Y, Cui YJ, Tang AM, Tang CS, Benahmed N. Changes in thermal conductivity, suction and microstructure of a compacted lime-treated silty soil during curing. *Eng Geol*. 2016;202:114-121. doi:10.1016/j.enggeo.2016.01.008
38. Zhou C, Ng CWW. A new and simple stress-dependent water retention model for unsaturated soil. *Comput Geotech*. 2014;62:216-222. doi:10.1016/j.compgeo.2014.07.012
39. Zhang F, Cui Y-J, Chen B. Investigation of suction effects due to stress release with compacted MX80 bentonite. *J Geotech Geoenvironmental Eng*. 2022;148:3-12. doi:10.1061/(asce)gt.1943-5606.0002849
40. Wang Q, Tang AM, Cui YJ, Barnichon JD, Ye WM. Investigation of the hydro-mechanical behaviour of compacted bentonite/sand mixture based on the BExM model. *Comput Geotech*. 2013;54:46-52. doi:10.1016/j.compgeo.2013.05.011
41. Kennedy J, Eberhart R. Particle swarm optimization. Proc. ICNN'95-international Conf. neural networks, vol. 4, IEEE; 1995:1942-1948.
42. Zhang Z, Ye WM, Liu ZR, Wang Q, Cui YJ. Mechanical behavior of GMZ bentonite pellet mixtures over a wide suction range. *Eng Geol*. 2020;264:105383. doi:10.1016/j.enggeo.2019.105383
43. Zhang Z, Ye W, Wang Q, Chen Y. Investigation on healing behavior of unsaturated GMZ bentonite pellet mixture based on compressibility. *Acta Geotech*. 2022;17:4461-4471. doi:10.1007/s11440-022-01494-9

How to cite this article: Yang JW, Cui YJ, Mokni N, Wang H. A triple-microstructure hydro-mechanical constitutive damage model for compacted MX80 bentonite pellet/powder mixture. *Int J Numer Anal Methods Geomech*. 2024;48:1654–1680. https://doi.org/10.1002/nag.3670

APPENDIX A

Due to the lack of data in Darde,[31] the initial dry density and initial void ratio of bentonite mixture (p_d and e_T) of Darde[31] were calculated with the masses and water contents of pellets and powder grains, by means of Equations (A1) and (A2).

$$m_s = \frac{m^{pellet}}{1 + w^{pellet}} + \frac{m^{powder}}{1 + w^{powder}} \tag{A1}$$

$$p_d = \frac{m_s}{V_v} \text{ and } e_T = \frac{p_s}{p_d} - 1 \tag{A2}$$

where m^{pellet} and m^{powder} are the initial masses of pellets and powder grains, which were 99.9 g and 39.5 g, respectively.[31] m_s is the total mass of pellets and powder grains in dry mass, w^{pellet} and w^{powder} are the water contents of pellets and powder grains, respectively, p_s is the density of soil particles, equal to 2.77 Mg/m^3.

The initial e_M^{intra} could be extracted from the MIP results of MX80 bentonite 7-mm pellet at initial state from this study and Molinero-Guerra et al.,[25] by accumulating the void ratio of pores with sizes larger than 1 μm. e_m^{intra} is the difference between e_T^{intra} and e_M^{intra} and e^{inter} is the difference between e_T and e_T^{intra}. Due to the lack of MIP results of Darde[31] for bentonite 7-mm pellet at initial state, the initial e_M^{intra} of this study was used instead, because the initial suctions, water contents and void ratios of the 7-mm pellets of this study and Darde[31] are almost the same (see Table 1).